RESEARCH

Study on dynamic mechanical response characteristics and fracture energy dissipation mechanism of sandstones with different saturations under real-time low temperature

Ming Li · Hao Yu · Jiazhi Zhang · Gang Lin · Lianying Zhang · Yanlong Chen · Fuqiang Zhu · Yiwen Mao · Hang Chen · Zhengbang Ding · Yihang Liang

Abstract It is of great significance to study the mechanical properties of rocks with different saturations for safe and efficient development of geotechnical engineering in low-temperature environments, such as open-pit mining and tunnel excavation in winter in cold areas, and etc. In this paper, the LT-SHPB test system was used to carry out impact loading tests for sandstones with various saturations at −20 °C environment. SEM was used to observe the cross-sectional characteristics of the specimens. The distributions of fragments were obtained by screening after impact failure. The energy dissipation model was established during the failure process. The research results indicated that the failure strength, elastic modulus, and peak strain of sandstones showed significant strain rate strengthening. Under the fixed strain rate, as the increase of the water content, the failure strength and elastic modulus and the sensitivity increased first and then decreased, while the peak strain showed the opposite change characteristics. 75% saturation was the turning point of the change. The sandstones under saturated water content exhibited remarkable ductile failure characteristics, while the brittle failure dominated in other conditions. The fundamental reason for this change was the difference between the freezing and frost heave effects of water-bearing specimens under low temperature conditions. The change characteristics of the macroscopic damage degree of sandstones with the strain rate and water content were basically the same as the characteristics of mechanical properties. The higher the internal density, the more the dissipated energy and surface specific energy for the whole failure of the specimen. The energy dissipation difference could directly change the macroscopic failure characteristics.

M. Li · Y. Chen
State Key Laboratory for Geomechanics and Deep Underground Engineering, China University of Mining and Technology, Xuzhou 221116, Jiangsu, China

H. Yu (✉) · F. Zhu · Y. Mao · H. Chen · Z. Ding · Y. Liang
School of Mechanics and Civil Engineering, China University of Mining and Technology, Xuzhou 221116, Jiangsu, China
e-mail: TS21030030A31@cumt.edu.cn

J. Zhang
State Key Laboratory of Coastal and Offshore Engineering, Dalian University of Technology, Dalian 116024, China

G. Lin
Laboratoire de Géologie, École Normale Supérieure, CNRS-UMR 8538, PSL Research University, 75231 Paris, France

L. Zhang
School of Civil Engineering, Xuzhou Institute of Technology, Xuzhou 221008, Jiangsu, China

Article Highlights

- The LT-SHPB test system was used to carry out impact loading tests for sandstones with various saturations at − 20 °C environment.
- SEM was used to observe the cross-sectional characteristics of the specimens. The distributions of fragments were obtained by screening after impact failure.
- The energy dissipation model of sandstones with different saturations at low temperatures was established during the failure process.

Abbreviations

A_0	Cross sectional area of the sample, mm^2
A_s	Cross section area of the pressure bar, mm^2
C_s	The propagation velocity of the stress wave in the compression bar, m/s
d_{iv}	The average of the maximum particle size and the minimum particle size within the i-th group of particle size range, mm
E_c	Elasticity modulus, GPa
E_d	Dynamic elastic modulus, GPa
E_s	Elastic modulus of the pressure bar, GPa
h	Height of the specimen, mm
L_0	Original length of the sample, mm
m_d	The mass of dry specimens, kg
m_f	Mass of a fully saturated specimen, kg
m_s	Specimen mass under various water contents, kg
n_i	Total number of equivalent spheres in the i-th particle size range
P	Impact pressure, MPa
r	Particle size coefficient, mm
r_i	Radius of the spheres in the i-th particle size range, mm
S	Saturation of the specimen, %
Std.	Standard deviation of the discrete value and the average value
S_ω	Surface area of all fragments after impact failure, cm^2
v	Impact velocity of the striker, m/s
V	Sound velocity of the, km/s
w	Water content of a fully saturated specimen, %
W_{iv}	The percentage of the mass of the i-th group of particle size fragments to the total mass of specimens, %
W_L	Dissipated energy, J
$\dot{\varepsilon}$	Strain rate
ε_c	Yield strain of the specimen
ε_d	Elastic strain of the specimen
ε_s	Peak strain of the specimen
$\varepsilon_I(t)$	Strain signals of the incident wave
$\varepsilon_R(t)$	Strain signals of the reflected wave
$\varepsilon_T(t)$	Strain signals of the transmitted wave

1 Introduction

More than 90% of open-pit coal capacity comes from cold climate regions above 38° North latitudes, such as Xinjiang, Inner Mongolia, North of Shaanxi Province and etc. Goal resources' safe and efficient mining faces enormous challenges under cold winter temperatures. There are two major influence factors. One is the water content in coal and rock masses. Drought risks are most likely to occur in North and Northwest areas with less precipitation and uneven distribution of groundwater system (Takarli et al. 2008; Guo and Shen 2016; Hu et al. 2019; Shen et al. 2020). Local springs or groundwater runoff are common during the open-pit mining process. At this point, the water contents of the open pit slope rock mass will significantly increase with uneven distributions (Li et al. 2014, 2021a; Zhang et al. 2021). In the low temperature in winter, the rock masses have different physical and mechanical properties in different water-bearing areas under the effects of freezing or frost heaving (Kodama et al. 2013; Wang et al. 2019a). The other is the high-strength mining blasting disturbance. A single blasting can yield 100 tons of coal resources for 10-million-ton open-pit mines. The high-intensity blast-induced stress waves have significant disturbance impacts on coal and rock mass (Navarro Torres et al. 2018; Chi et al. 2019; Shen et al. 2020; Azizi and Moomivand 2021). Therefore, the study on the mechanical properties of frozen sandstones and the damage and fracture mechanism under impact loads is essential to efficiently ensure the safe and efficient mining of open-pit coal mines in winter. The blasting mining of coal seams can be realized by reasonably designing blasting parameters. On the other hand,

it can provide references for the design of control parameters of the stability of the slope coal and rock masses. Besides the large-scale open-pit coal mines, such problems also occur in other engineering in winter in northwestern and northern China, such as tunnel excavation, foundation excavation of large buildings, etc. (Cui et al. 2020; Jiang et al. 2021).

Water is one of the fundamental environmental factors faced by rocks (Cai et al. 2020b). Rocks will undergo weathering and decomposition after long-term exposure to air under natural environmental conditions, which will cause changes in physical and mechanical properties that are stable in a short period (Shang et al. 2004; Qi et al. 2009; Jaques et al. 2020). However, soaked in water or aqueous state, the clay mineral particles in rocks will show significant swelling. In addition, some mineral components readily soluble in water dissolve in water. This can cause remarkable changes in the internal structures of rocks and, in turn affect the macroscopic physical and mechanical properties. Such changes are more evident for sedimentary rocks such as coal-measure strata (Hale and Shakoor 2003; Deng et al. 2016; Kim and Changani 2016). The low-temperature environment is one of the essential factors affecting the mechanical properties of water-bearing rocks. Water can change from the liquid phase into solid phase as the temperature changes from room temperature to below 0 °C. The volume growth will result in significant changes in the microstructure characteristics of rocks (Al-Omari et al. 2015; Huang et al. 2021). When the water content is within a specific range, rocks are frozen and their mechanical properties will be strengthened, due to the contraction of particles and loads of pore ice (Zhou et al. 2021; Ming et al. 2021). When the water content exceeds the maximum value of the range, rocks will undergo frost heaving. Their physical and mechanical properties are significantly affected during water migration and accumulation in freezing zones. Huang et al. (2018) have pointed out that rocks with water contents of over 9% will experience significant frost heaving. There are plentiful research results on the static mechanical properties of rocks in the low-temperature environment (Bayram 2012; Bai et al. 2020; Deprez et al. 2020). Scholars have systematically studied mechanical characteristic parameters of different types of rocks, such as failure intensity, elastic modulus, macro failure characteristics and etc. (Feng et al. 2018b; Zhang et al. 2018;

Wang et al. 2019a). The variations of mechanical properties of rocks with temperature and water content have also been discussed (Dwivedi et al. 2000; Kodama et al. 2013; Jia et al. 2020).

The problems of rock dynamics are gradually increasing in the low-temperature environment with the increase of geotechnical engineering in cold regions, which restrict the safe and efficient development of engineering. Scholars have conducted research on the rock mechanics characteristics under low-temperature environment by using the split-Hopkinson pressure bar (SHPB) test system and the corresponding low-temperature loading devices (Wang et al. 2016a; Yang et al. 2019; Weng et al. 2020). The results indicated that as the loading rate increased, the mechanical strength and dynamic elastic modulus of rocks increased significantly under fixed temperature and physical properties, which are the same as the research results at room temperature (Ma et al. 2018; Ke et al. 2018). The temperature loading conditions are one of the critical factors in researching rock dynamic characteristics under low-temperature environments. In the natural water-bearing state dynamic mechanical properties of rocks occur temperature strengthening as the environmental temperature increases, and the degree of temperature strengthening is related to the type of rocks (Wang et al. 2019b; Yang et al. 2019; Weng et al. 2020). It is worth noting that the current research focuses on the dynamic mechanical characteristics of rocks under freeze–thaw cyclic loading (Luo et al. 2020; Li et al. 2021b). The research results showed that as the number of freeze–thaw cycles increased, rock's dynamic strength and dynamic elastic modulus would decrease. This was mainly caused by the changes in rock pore structures under freeze–thaw cycles (Zhang et al. 2018; Seyed Mousavi et al. 2019; Zhou et al. 2020b). In order to explore meso-mechanism of rock macroscopic and dynamic mechanical properties under low-temperature environments, many mesoscopic test methods have been adopted, such as NMR, CT technology, mercury intrusion, etc. (Zhou et al. 2015; Chen et al. 2021). Moreover, the establishment of some theoretical models and the analysis of energy dissipation mechanisms can also provide theoretical support for the study of macroscopic and dynamic mechanical properties change of rocks
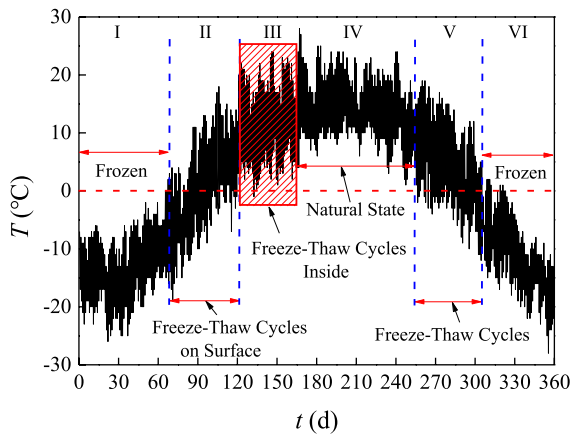
Fig. 1 Temperature variation characteristics of Beitashan Pasture Coal Mine in Xinjiang, China, in 2018 (north latitude 44° 59′ 20″–45° 33′ 20″ and east longitude 90° 16′ 45″–91° 11′ 48″)

Fig. 2 Characteristics of frozen rock-soil mass around the open-pit mine slope spring

under low temperature environment (Wang et al. 2016b, 2017; Wang et al. 2019c).

The safety of engineering construction in coal regions is of great significance in winter. As shown in Fig. 1, the rock-soil masses are in freezing period for nearly 1/3 of the year (120 days). Therefore, the key to efficient open-pit coal mining in winter is to clarify the mechanical response characteristics of frozen rocks under the blast and impact loadings. Meanwhile, clarifying the damage and fracture mechanism of frozen rocks under the blasting disturbance is the key to slope safety protection during the blasting mining process. As shown in Fig. 2, open-pit mining may

encounter water-rich areas such as springs. The rock mass has saturated water content in the spring areas. The water content will gradually decrease because it is far from the spring area. The change in the water content is the major reason for different rock dynamic mechanical response under low temperature environment. Taking the winter blast mining of Beitashan Pasture Coal Mine in Xinjiang as the research background and the average winter temperature of −20 °C as the test temperature, this paper will carry out experiments on mechanical properties of sandstone specimens with various water contents under different impact loads by using the LT-SHPB test system. Then based on the energy dissipation theory, it will study the mechanical properties of frozen sandstone under impact loads, the mesoscopic fracture mechanism and the energy dissipation mechanism of macroscopic failure using the SEM test system. The research results are aimed to provide references for open-pit mining in cold regions, blasting and construction of similar geotechnical engineering and the design of rock-soil mass protection parameters.

2 The testing scheme

In this testing, the real-time low-temperature SHPB (LT-SHPB) test system was adopted to perform real-time impact compression tests on sandstone specimens with different saturations under low-temperature conditions. There were two processes. Firstly, the processed sandstone specimens were treated with different saturations. Then the impact loading tests were conducted in low temperature environment.

2.1 Specimen preparations

2.1.1 Sandstone specimen preparation

In this testing, the sandstones were taken from the southern slope of Beitashan Pasture Coal Mine in Xinjiang. By X-ray diffraction analysis technology, the main mineral components are quartz (54.6%), muscovite (29.3%), Kaolinite (8.9%), borated muscovite (2.9%) and montmorillonite (4.3%). According to the recommendations on rock dynamics test from the International Society for Rock Mechanics (ISRM), sandstones were processed into cylindrical samples with the dimension of 50 × 50 mm after

coring, cutting and grinding, which could meet the requirements of flatness (≤ 0.05 mm) and parallelism (≤ 0.02 mm) at both ends (Zhou et al. 2012; Zhang and Zhao 2014). The basic physical and mechanical parameters of the standard specimens are shown in Table 1.

2.2 Treatment of water saturation in specimens

The definition of saturation (water saturation) is given as follows (Liu et al. 2020b):

$$S = \frac{m_s - m_d}{w} \times 100\% \tag{1}$$

where S is the saturation of the specimen; m_s is the specimen mass under various water contents; m_d is the mass of dry specimens; w is the water content of a fully saturated specimen, which can be calculated by Eq. (2).

$$w = \frac{m_f - m_d}{m_d} \times 100\% \tag{2}$$

where m_f is the mass of a fully saturated specimen.

The sandstone specimen saturation treatment process is specified in relevant regulations of ISRM on rock saturation test. Firstly, the specimens shall be wholly dried to eliminate the uneven water content of the specimens. Secondly, the dried specimens are completely saturated. Finally, the saturated specimens were prepared into specimens with various saturations. In this testing, the specific process is as follows (Liu et al. 2020b; Huang et al. 2021):

1. Drying treatment: The DHG9076 electric constant-temperature drying oven was used for dying of specimens at 105 °C for 24 h. After 24 h, the specimen was weighed every 1 h until the weight difference was less than 0.02 g. Next, all dried specimens were taken out and put into dryers.

The specimens were cooled to room temperature and sealed with bags.

2. Saturation treatment: The dried specimens were put into the negative vacuum pressure air extracting devices. The vacuum pumping was performed for 6 h at an air pressure of -0.09 MP. Then the distilled water was injected with the negative pressure in the sealed tank. The injection stopped until the distilled water level was higher than the specimen. In the beginning, a large number of bubbles floated on the surface of the specimen. After standing for some time, the bubbles disappeared. At this point, the air pressure in the container was adjusted to the atmospheric pressure. After soaking for 6 h, the moisture on the surface was dried every half an hour. The specimen was difference until the weight difference between two weighings was less than 0.02 g. Finally, the specimens were wrapped in plastic and put into sealed bags.

3. Saturation treatment: According to Eqs. (1) and (2), the average saturation of the sandstone specimens in fully saturated states could be calculated. Then the specimen mass could be obtained under the saturations of 25%, 50% and 75%, respectively. Finally, the processed specimens were dried in a drying box at a temperature of 50 °C. The mass m_s was weighed every 1 min. The drying of the entire group of specimens was completed when m_s reached the target saturation level.

The prepared specimens with various saturation were wrapped in plastic wrap, sealed with tape and put into the curing box for the impact test (Weng et al. 2021).

Figure 3 shows the process flow of the specimen saturation treatment and low-temperature treatment.

2.3 The system and principles of low-temperature impact testing of sandstones

The real-time LT-SHPB was adopted for the impact test, as shown in Fig. 4. The whole system is mainly composed of low-temperature loading, impact loading and drive, pressure bar, data acquisition and processing, and energy absorption systems.

The low-temperature loading system can provide low-temperature loads for specimens, which can be
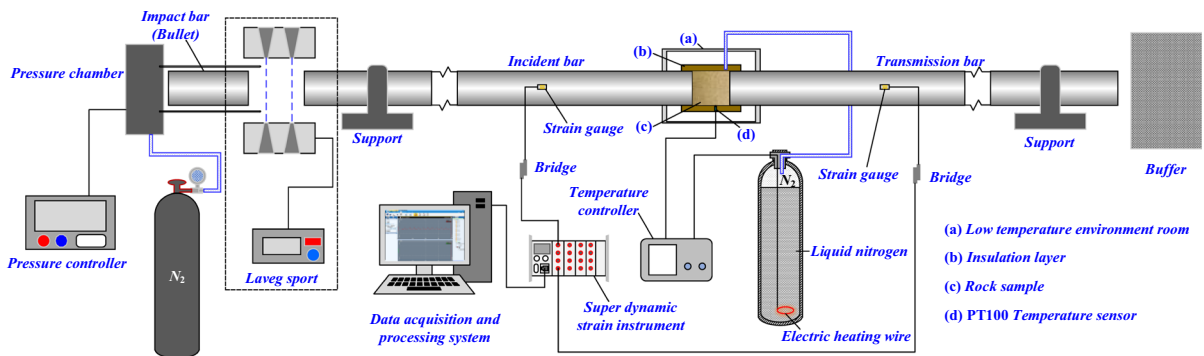
Table 1 Basic physical and mechanical properties of sandstone samples

σ_c (MPa)	E_c (GPa)	V (km·s^{-1})	ρ (kg·m^{-3})	μ
45.14	4.59	2.819	2283	0.165

σ_c-compressive strength; E_c-elasticity modulus; V-sound velocity; ρ-density; μ-Poisson's ratio
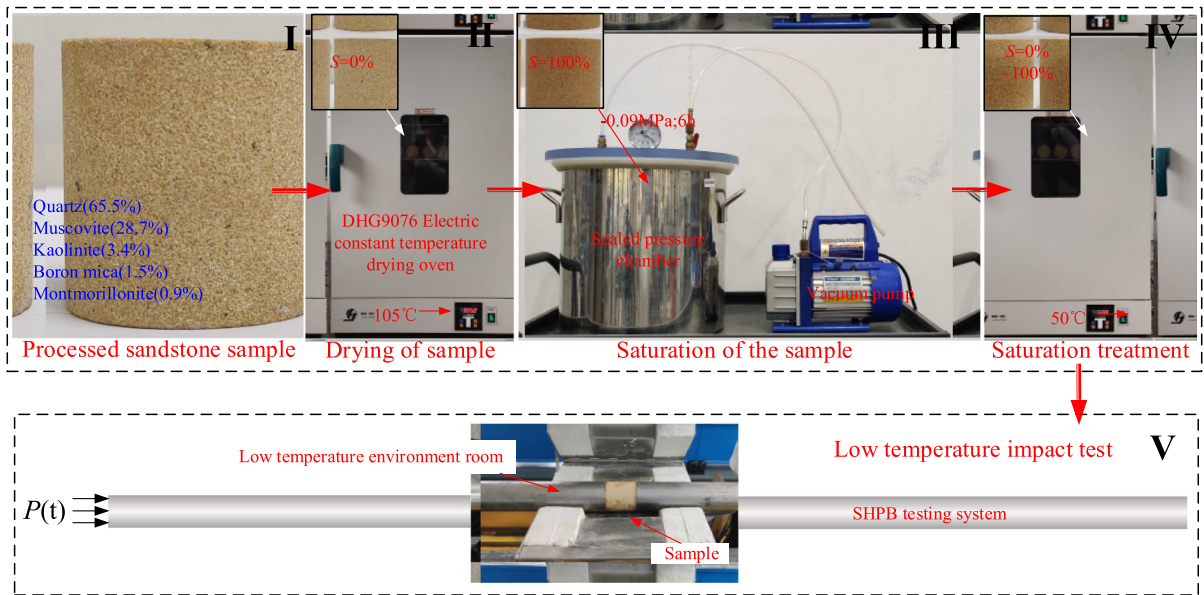
Fig. 3 Process flow of the specimen saturation treatment and low-temperature treatment

Fig. 4 Real-time low temperature rock dynamic mechanics test system

impacted under real-time low-temperature conditions. The low-temperature loading system contains the low temperature controller, liquid nitrogen container, heating wire, low temperature sensor and low temperature environment room. The aluminum silicate needle blanket was adopted in the low temperature environment room to form the insulating layer, which could ensure the minimum temperature of -50 °C. During the test, the liquid nitrogen in the container was vaporized into nitrogen under the action of the thermocouple, and flowed into the low-temperature chamber to reduce the temperature of the specimen.

The heating wire stopped working when the room temperature detected by the low-temperature sensor reached the preset value. The process was automatically controlled by the solenoid valve. The thermocouple could automatically restart when the room temperature exceeded the preset value. The test results indicated that the room temperature could stay at the preset value, and the temperature difference was within ± 0.2 °C.

Except for the low-temperature loading system, the composition and functions of the other four systems were the same as those of the conventional

SHPB test system. During the test, specimens were installed between the incident bar and the transmitted bar according to the test plan. The low-temperature environment room was adjusted to the corresponding temperature, which was kept for 6 h. Then the impact loading was conducted according to the plan. The high-pressure nitrogen drove the striker to hit the incident bar during impact loading. Thus the incident waves were generated and transmitted to the specimen along the incident bar. Part of the incident waves was reflected to the incident bar to form the reflected waves, and the other part was transmitted through the specimen to the transmission bar to form the transmitted waves. In the process, the strain signals were collected by the strain gauge, transmitted to ultra-dynamic strain gauge, and finally saved to the computer.

According to the one-dimensional theory of stress waves, the specimen's stress σ, strain ε and strain rate $\dot{\varepsilon}$ could be calculated by the three-wave method, as follows (Lifshitz and Leber 1994; Xia and Yao 2015; Xu and Dai 2018):

$$\begin{cases} \dot{\varepsilon} = \frac{C_s}{L_0}\left[\varepsilon_I(t) - \varepsilon_R(t) - \varepsilon_T(t)\right] \\ \dot{\varepsilon} = \frac{C_s}{L_0}\int \left[\varepsilon_I(t) - \varepsilon_R(t) - \varepsilon_T(t)\right]dt \\ \sigma = \frac{A_s}{2A_0}E_s\left[\varepsilon_I(t) - \varepsilon_R(t) - \varepsilon_T(t)\right] \end{cases} \quad (3)$$

where C_s is the propagation velocity of the stress wave in the compression bar; $\varepsilon_I(t)$, $\varepsilon_R(t)$ and $\varepsilon_T(t)$ refer to the strain signals of the incident wave, the reflected wave and the transmitted wave, respectively. E_s is the elastic modulus of the pressure bar; A_s is the cross section area of the pressure bar; A_0 is the cross sectional area of the sample; L_0 is the original length of the sample.

The test temperature was set at -20 °C to simulate the average winter temperature in Xinjiang. Five groups of specimen saturation were set, that is 0%, 25%, 50%, 75% and 100%. Five groups of impact loads were designed, that is 0.3 MPa, 0.4 MPa, 0.5 MPa, 0.6 MPa and 0.7 MPa. During the test, the saturation and impact load were taken as change factors, and the orthogonal experiment was carried out.

During the test, in order to ensure that test could satisfy two assumptions, the rubber sheet was used as the waveform shaper (Yin et al. 2015; Lin et al. 2021). The improved waveforms are shown in Fig. 5. It could be seen that the superposition of the incident
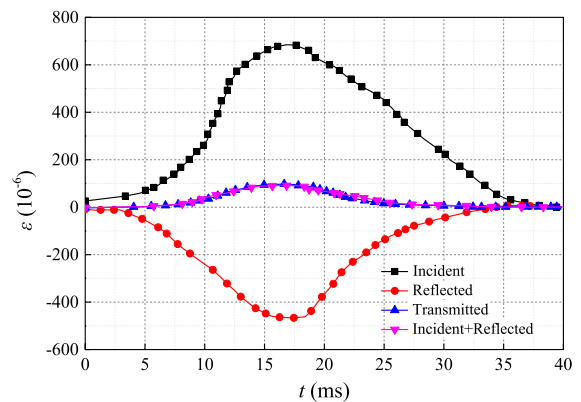

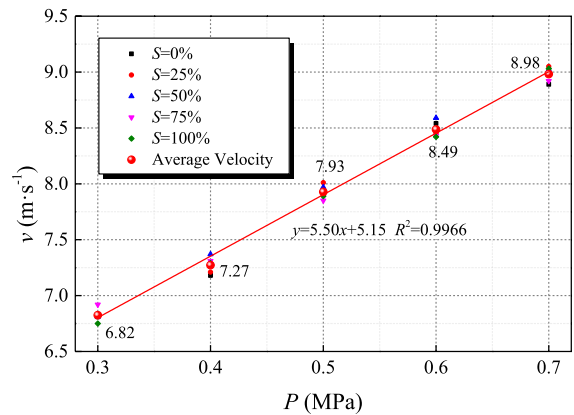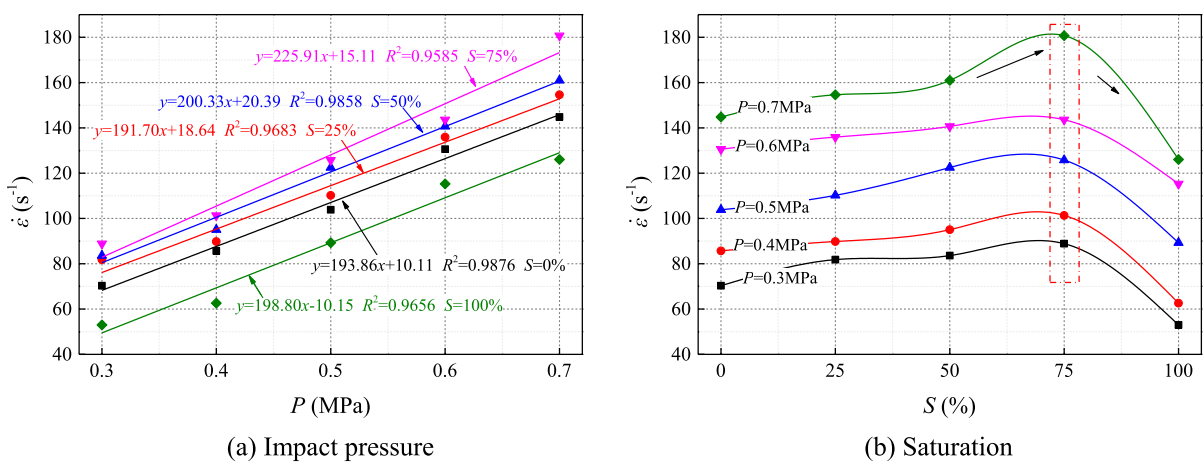**Fig. 5** Waveforms in the impact loading test

Fig. 6 Variation curves of impact velocity with the impact pressure

wave and the reflected wave coincides with the transmitted wave, indicating that the test could satisfy the assumption of uniformity. Then the incident wave was stable and the growth time was long, which could provide enough time for the constant stress of two ends inside the specimen. Finally, the three groups of waveforms presented the shape of half sine waves. The waveforms were relatively smooth without obvious transverse oscillations. The test could better meet the one-dimensional stress wave propagation hypothesis (Li et al. 2016, 2017).

The laser velocimeter obtained the change laws of the striker impact velocity v with loaded impact pressure P for different specimens during the testing, as shown in Fig. 6. The striker impact velocity has nothing to do with the states of rock specimens. In Fig. 6,

the loading and output of the overall equipment were relatively stable. As P increased, v increased rapidly and linearly. As P increased from 0.3 to 0.7 MPa, v increased from 6.82 to 8.98 m/s. According to Eq. (6), the change laws of strain rates $\dot{\varepsilon}$ with the impact pressure P and the saturation S were obtained under different conditions, as shown in Fig. 7. In Fig. 7a, as P increased, $\dot{\varepsilon}$ increased rapidly and linearly, and the slope of the line gradually changed with the increase of S. When S increased from 0 to 75%, the linear slope continued to increase, indicating that the sensitivity of $\dot{\varepsilon}$ to P gradually enhanced. When S increased from 75 to 100%, the linear slope was greatly reduced, and the sensitivity of $\dot{\varepsilon}$ to P decreased rapidly. With the increase of saturation, $\dot{\varepsilon}$ first increased and then decreased. When S was 75%, $\dot{\varepsilon}$ reached the maximum value, as shown in Fig. 7b. Figure 7 showed that the saturation significantly impacted the strain rate, which was directly related to the freezing and frost heave of specimens with different water contents in low-temperature environments.

In the following analysis, the change in the mechanical properties of sandstones will be analyzed with the strain rate as an independent variable. The failure characteristics and energy dissipation mechanism are related to the energy input, that is, the initial velocity of the striker. Therefore, the striker velocity will also be taken as an independent variable for relevant conclusion analysis (Wang et al. 2020b).

3 Dynamic mechanical response characteristics and microscopic mechanism of frozen sandstones with different saturations

3.1 Dynamic stress–strain curve change characteristics of frozen sandstones

The complete stress–strain curves of frozen sandstone specimens with different saturations at different strain rates were obtained through an impact loading test, as shown in Fig. 8a–e. In order to further compare the influence of saturation on the dynamic stress–strain curves of frozen sandstones, the dynamic stress–strain curves with different saturations at similar strain rates were given, as shown in Fig. 8f. The strain rates were similar, so the loading strain rates were assumed to be the same in the analysis.

Based on the characteristics of each stress–strain curve in Fig. 8, a typical stress–strain curve of frozen sandstone was obtained under a high strain rate, as shown in Fig. 9. It could be seen that the deformation of the frozen sandstone at low temperatures underwent the compaction stage, elastic deformation stage, plastic deformation stage and post-peak attenuation stage under the action of high strain rate loads. In Fig. 8a–e, with the same saturation, the stress–strain curves of frozen sandstone with different strain rates indicated that the changes in strain rate didn't change the basic deformation characteristics of the curves, but could significantly change
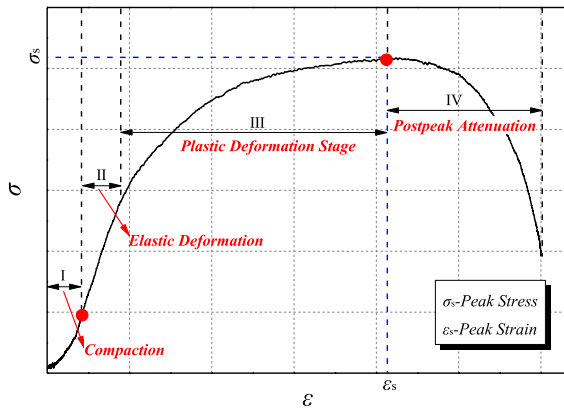

Fig. 7 Variation curves of strain rates with the impact pressure and saturation
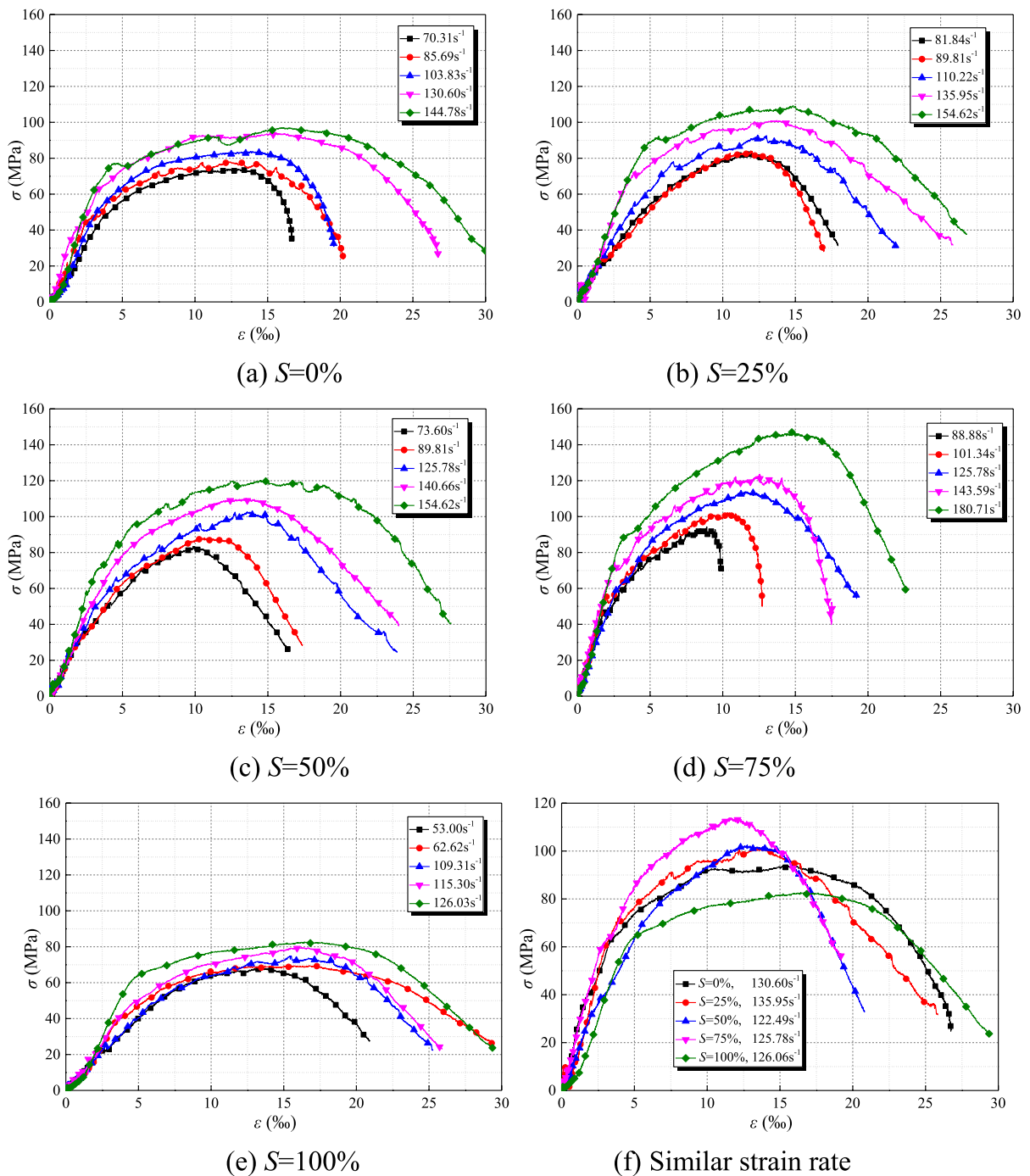
Fig. 8 Dynamic e stress–strain curves of frozen sandstones under different conditions

the characteristic dynamic parameters of sandstones, such as peak strain, peak stress and dynamic elastic modulus. In Fig. 8f, under the same strain rate, the stress–strain curves of the frozen sandstones with

the saturation of 0 and 100% experienced remarkable compaction stage, In contrast, the other three sets of curves' compaction stages were shorter or did not exist (Wang et al. 2019a). Additionally, the saturation

Fig. 9 Dynamic stress–strain curves of frozen sandstones

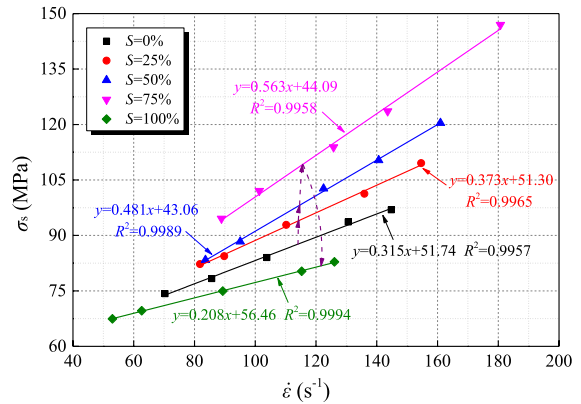**Fig. 10** Variation curves of the dynamic compressive strength of frozen strength

significantly changed the dynamic mechanical parameters of frozen sandstones.

3.2 Variation laws of dynamic mechanical characteristic parameters of frozen sandstones

In Figs. 8 and 9, both the strain rate and saturation of specimens significantly impacted the mechanical properties of sandstone. The quantitative analysis was conducted to clarify the specific changes. According to the complete stress–strain curves, the variation laws of the sandstone dynamic compressive strength (peak strength) σ_s, dynamic elastic modulus E_d and peak strain ε_s were obtained and illustrated, respectively.

3.2.1 Dynamic compressive strength change characteristics

Figure 10 shows variation laws of frozen sandstone's dynamic peak strength σ_s with the strain rate $\dot{\varepsilon}$ under different saturations S. Under various S, as $\dot{\varepsilon}$ increased, σ_s increased rapidly and linearly, showing significant strain rate strengthening. Under five sets of saturations, when $\dot{\varepsilon}$ increased from the minimum to the maximum, σ_s increased by 30.56% ($S=0\%$, σ_s from 74.24 to 96.93 MPa), 33.19% ($S=25\%$, σ_s from 82.25 to 109.54 MPa), 44.43% ($S=50\%$, σ_s from 83.37 to 120.41 MPa), 55.45% ($S=75\%$, σ_s from 94.55 to 146.98 MPa) and 22.83% ($S=100\%$, σ_s from 67.44 to 82.84 MPa), respectively. The overall growth rate firstly increased and then decreased. With S of 75%, σ_s was mostly affected by the increase of $\dot{\varepsilon}$. The

scope of $\dot{\varepsilon}$ was different during the loading process, so it is not objective to use the variation amplitude to judge the effects of the saturation on the compressive strength. Therefore, the relationships between dynamic compressive strength and strain rate were linearly fitted, as shown in Fig. 10. It could be found that as S increased, the linear slope first increased and then decreased. When S was 75%, the linear slope was the largest. The linear slope represented the sensitivity of the dynamic compressive strength of frozen sandstones to the strain rate. Within the same strain rate change range, the larger the slope, the greater the increasing amplitude of the dynamic compressive strength, the greater the sensitivity of dynamic compressive strength to the strain rate. It is particularly noteworthy that, within the same strain rate range, when S increased from 0 to 75%, σ_s gradually increased. While S increased from 75 to 100%, σ_s was greatly reduced. With S of 100%, σ_s was much smaller than that under other saturations. The change in the dynamic compressive strength was the same as the change in the sensitivity, which was mainly affected by the internal cracks of frozen sandstone with different saturations and ice.

3.2.2 Variation characteristics of dynamic elastic modulus

According to the slopes of the complete stress–strain curves at the elastic stage, frozen sandstone's dynamic peak strains were obtained under different conditions. Figure 11 gives variation curves of the dynamic
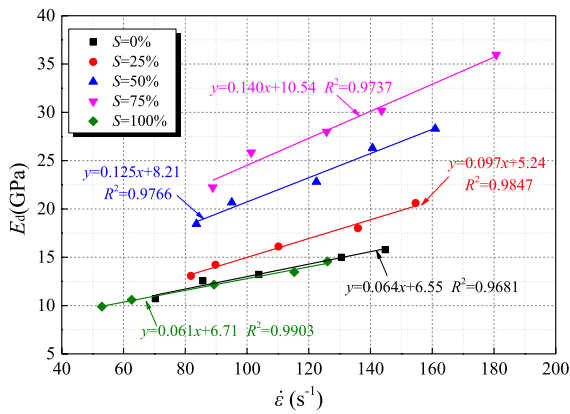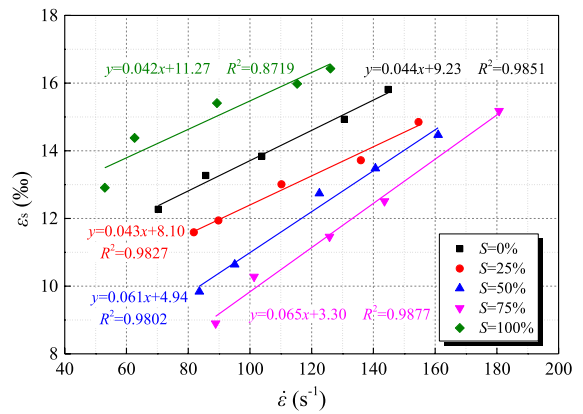
Fig. 11 Variation curves of the dynamic elastic modulus of frozen sandstones

Fig. 12 Variation curves of the dynamic peak strain of frozen sandstones

peak strain rates. The variation law of the dynamic elastic modulus was consistent with the compressive strength, presenting great strain rate strengthening. Specifically, under five sets of S, E_d increased by 47.31% ($S=0\%$, E_d from 10.71 to 15.78 GPa), 57.64% ($S=25\%$, E_d from 13.07 to 20.60 GPa), 53.43% ($S=50\%$, E_d from 18.45 to 28.30 GPa), 61.76% ($S=75\%$, E_d from 22.23 to 35.96 GPa) and 47.29% ($S=100\%$, E_d from 9.89 to 14.57 GPa), respectively. Meanwhile, the comparison between Figs. 7 and 8 indicated that the effects of saturation on the dynamic elastic modulus and dynamic compressive strength of frozen sandstones were the same. The sensitivity of dynamic elastic modulus to the strain rate increased first and then decreased with the increase of saturation. The changing trend was also true with the same range of strain rate. When S was 75%, E_d and σ_s were the highest. The change characteristics of the dynamic elastic modulus of frozen sandstones were also closely related to internal cracks of frozen sandstones with various saturations.

3.2.3 Variation characteristics of the dynamic peak strain

According to the coordinates of the peak points of the stress–strain curves, the dynamic peak strain ε_s of frozen sandstones were obtained under different loading conditions and saturations. Figure 12 shows the change curves of the dynamic peak strain with the strain rate. The change characteristics were the same as those of the former two

parameters. As $\dot{\varepsilon}$ increased, ε_s increased linearly and rapidly. Under five sets of saturations, ε_s increased by 28.85% ($S=0\%$, ε_s from 12.27 to 15.81‰), 28.13% ($S=25\%$, ε_s from 11.59 to 14.85 ‰), 47.05% ($S=50\%$, ε_s from 9.84 to 14.47‰), 70.56% ($S=75\%$, ε_s from 8.90 to 70.56‰) and 27.27% ($S=100\%$, ε_s from 12.91 to 16.53‰), respectively. The comparison of curves indicated that within the exact scope of $\dot{\varepsilon}$, as S increased, ε_s decreased first and then increased. When S was 75%, ε_s was the smallest, opposite to the changes of σ_s and E_d. The relationships between the dynamic peak strain and the strain rate were fitted. After fitting, the linear slope first increased and then decreased with the increase of saturation. The maximum slope was at 75% saturation, indicating that the sensitivity of ε_s was the strongest at this point. The value of ε_s was related to the entire deformation process before the peak. Therefore, internal cracks were the main reason for the difference in the dynamic peak strain.

3.3 Characteristics of dynamic brittle-ductile transition of frozen sandstones

Sandstone is a typical brittle material. It will exhibit significant ductility characteristics under external loads and environmental conditions (Liu et al. 2020a; Walton 2021). Compared with brittleness, ductility refers to the rock material having prominent plastic deformation characteristics before failure. Therefore, the ratio of the peak and yield strain could be used as

the dynamic brittle-ductile parameter of frozen sandstone. The specific equation is as follows (Ai et al. 2016; Tarasov and Potvin 2013):

$$\lambda = \frac{\varepsilon_s}{\varepsilon_c} \tag{4}$$

where λ is the dynamic brittle-ductile parameter; ε_s is the peak strain, and ε_c is the yield strain.

Equation (4) could be used to determine the value of λ. The most critical issue was determining the stress–strain curve's yield point. According to the characteristics of the complete stress–strain curve of the frozen sandstone, the method in Fig. 13 was adopted to fix the yield point. Firstly, the fitting straight line (Line I) was fixed at the linear elastic stage. The peak point was taken as the reference point. Line II was parallel to Line I, intersecting the abscissa at point A. Secondly, according to the coordinates of point A, the values of ε_d could be obtained. Finally, taking the abscissa 0 points as the starting point, and ε_d as the gauge length, Line l was made parallel to the ordinate axis. The intersection of Line I and the stress–strain curve was the yield point, corresponding to the yield strain of ε_c and the yield stress of σ_c.

In Fig. 13, according to the characteristics of the stress–strain curve, the frozen sandstone entered the plastic deformation stage before the yield point. The strain from the end of the elastic stage to the yield point was the initial compaction strain. After the yield point, the frozen sandstone entered the microcrack propagation stage. According to statistics, the ratio of sandstone yield strain to peak strain was between 73 and 78% under various conditions, so 75% of the peak stress was uniformly taken as the yield point. According to Eq. (4), λ was 1.33 in a completely brittle state.

According to the stress and strain data, λ could be obtained under various conditions. Figure 14 shows the change curves of λ with the saturation. The discrete value of λ was dynamic, corresponding to each saturation. It could be seen that the strain rate slightly affected λ. Therefore, the average dispersion value could be taken as λ. Std. was the discrete and average values' standard deviation. $Std./_{s=75}$ refers to the standard deviation between λ and the average value under various strain rates and S of 75%. In Fig. 14, the sandstones with different saturations exhibited significant toughness under impact load under low temperature environment. As S gradually increased, λ decreased first and then increased. As S increased from 0 to 75%, λ decreased from 2.71 to 2.09, with a decreasing amplitude of 22.88%. The brittleness of frozen sandstone was enhanced. As S increased from 75 to 100%, λ increased from 2.09 to 4.29, increasing by 1.05 times. At this point, the dynamic toughness of frozen sandstone was quickly strengthened. Meanwhile, the standard deviation and saturation were positively correlated. With the increase of S, the standard deviation gradually increased, proving that strain rate's influence on ductile–brittle characteristics was gradually increasing (Xue et al. 2014).
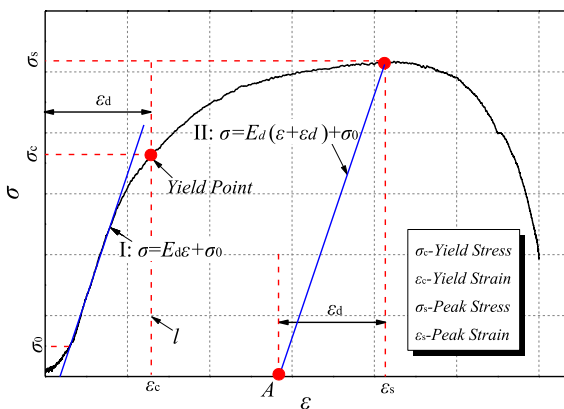
Fig. 13 Method of determining yield point of the dynamic stress–strain curve of frozen sandstone
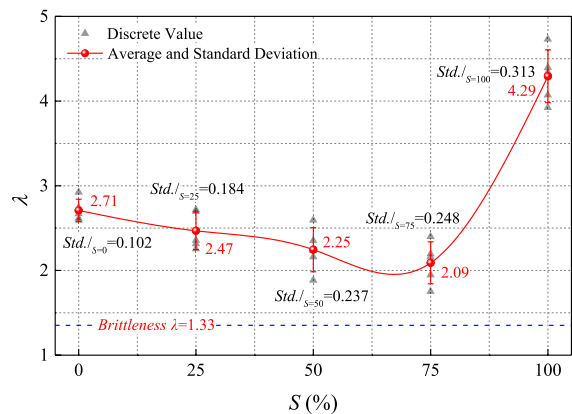
Fig. 14 Variation curves of the dynamic ductile–brittle coefficient with the saturation

3.4 The mesoscopic mechanism of dynamic mechanical response characteristics of frozen sandstone

3.4.1 The micromechanical behavior of water-bearing sandstone in low-temperature environment

The change laws of the mechanical properties of frozen sandstone indicated that there were apparent strain rate strengthening effects under the same saturation, which is the same as the conclusions of a large number of existing studies (Yang et al. 2019; Weng et al. 2020). In fact, after fixing the environmental conditions and the rock's conditions, the rock's mechanical properties show significant strain rate strengthening effects under the impact load (Wang et al. 2019b).

Within the same range of strain rate and under low-temperature environments, the influence of saturation on the dynamic mechanical properties of sandstone can be summarized in two stages. As S increased from 0 to 75%, the strength characteristics (peak stress) and stiffness properties (elastic modulus) showed significant saturation strengthening effects. As S increased from 75 to 100%, the saturation weakening effects existed. Figure 15 gives the reasons for such changes. In the original state, the internal microstructure of sandstone was mainly divided into the rock matrix and cracks, pre-existing cavity and free and crystal water. After completely dried, the sandstone only contained the rock matrix, cracks, and pre-existing cavity, as shown in Fig. 15a. During the saturation treatment process, clay minerals such as kaolinite and montmorillonite in the sandstone swelled with water. Thus the cracks and primary cavities were reduced in dimension (Cherblanc et al. 2016; Wang et al. 2021b). Some smaller cavities were closed, as shown in Fig. 15b. After the saturation treatment, the low-temperature treatment of sandstones had two situations: freezing enhancement and frost heave weakening of the mechanical properties. It is well known that the same water quality increased by about 9% in volume after freezing (Huang et al. 2020; Song et al. 2021). The water inside the sandstone was frozen under low saturation. The ice filled the original cracks in the sandstone and acted as the binder for the rock matrix on both sides of the cracks. Meanwhile, the freezing load could effectively reduce the internal porosity of

the sandstone. In Fig. 15c, some primary pores in the matrix were filled with ice, and their mechanical properties were greatly enhanced. The enhancement efficiency gradually increased with the increase of saturation (Lin et al. 2021). Under fully saturated conditions, the volume expansion of water after freezing into ice caused extreme frost-heaving load inside the crack and the dimension of the crack increased (Tan et al. 2018; Li et al. 2018; Ke et al. 2021; Wang et al. 2021a). At the same time, new cracks occurred and penetrated the original cracks, as shown in Fig. 15d. The frost heaving caused the internal porosity of the sandstone to increase and the mechanical properties to decrease significantly.

In order to further illustrate the impact of saturation on the meso-mechanical behavior of sandstone in a low-temperature environment, scanning electron microscopy (SEM) was used to observe the internal micro-structure characteristics of sandstone, as shown in Fig. 16. The observed sections were formed by mechanical cutting and were not subject to impact tests. At a magnification of 100 times, the specimens with different saturations had significant differences after being treated at low temperatures. Under arid conditions ($S = 0\%$), there were a lot of primary defects in the sandstone, including the penetrating cracks and independent cavities free in the rock matrix (Cai et al. 2020a). There were cracks and voids when S was 25%, tbut the dimensions were smaller. Besides, crack closures due to expansion could be observed locally. Large-scale cracks were not observed with S of 20% and 75%. The internal structure of the sandstone was nearly complete, and the porosity was more minor due to the saturated expansion and the binding load of ice. When S was 100%, many frost heave cracks and regionally distributed frost heave defects were caused inside the specimens after the low temperature. Thus, the changes in internal cracks and the effects of freezing loads and frost heave loads were the fundamental reasons for the dynamic meso-mechanical changes of sandstones with different saturations in low-temperature environments (Zhou et al. 2020a).

3.4.2 Mesoscopic characteristics of dynamic fracture of frozen sandstone

SEM was used for frozen sandstone sections with different saturations after dynamic failure. In order to
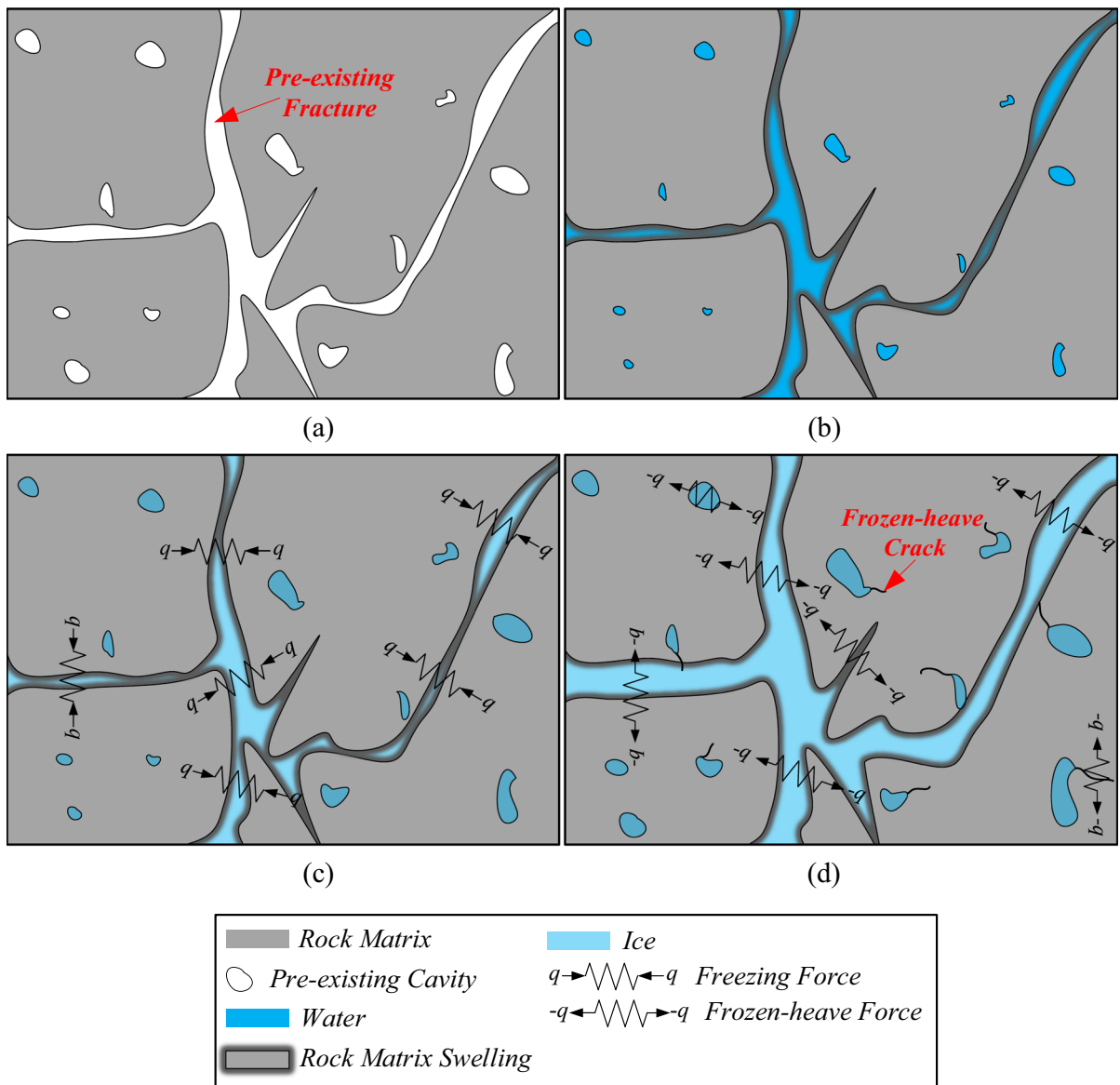
Fig. 15 Schematic diagrams of micromechanical behavior of sandstone in low-temperature environment (a. Primary structure of the sandstone; b. Saturation treatment; c. Mechanical behaviors under low saturation; d. Mechanical behaviors under complete saturation

analyze the meso-fracture characteristics of the sections more clearly, the observation images magnified 2000 times were selected, as shown in Fig. 17. After impact failure, the sections of frozen sandstones with different saturations showed apparent differences. When S was 0%, the sandstone fractures were dominated by brittle cleavage steps with slight ductile slippage. There were prominent stripe zones at the upper left, which were formed by the displacement of the

rock matrix on both sides under the action of impact load. When S was 25%, 50% and 75%, the sandstone fracture belonged to brittle fracture. The cleavage step entirely occupied the cross-sections of specimens. Some exposed grains were left by brittle fractures and brittle cracks with relatively flat edges. When S was 100%, the cross-sections were nearly all flexible dislocation strips. Dimples could be observed locally with elliptical shapes and superior ductility.
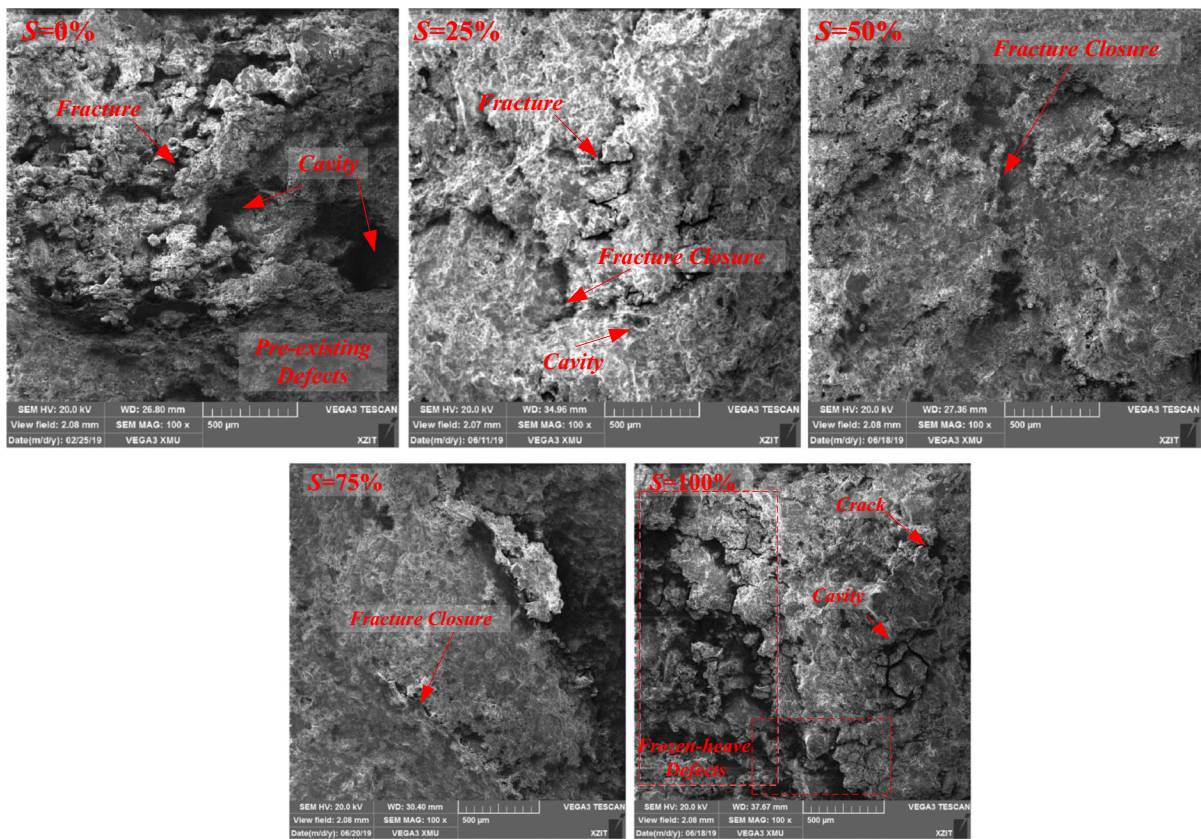
Fig. 16 Meso characteristics of the internal structure of sandstone with different saturation (100 times)

In the process of brittle fracture, the input energy of external load was mainly used for brittle deformation, and the strength and rigidity of sandstone were high. While ductile fracture, the input energy was consumed in internal plastic deformation, leading to low overall strength and stiffness of specimens. The plastic deformation was significantly increased (Xie et al. 2011; Wang et al. 2020a).

4 Impact failure characteristics and energy consumption mechanism of frozen sandstone with different saturations

4.1 Impact failure characteristics of frozen sandstone

4.1.1 Variation laws of impact failure characteristics

After the impact loading test, the fragments of frozen sandstone under different impact velocities and saturations were collected, as shown in Table 2. The fragments of sandstone specimens were completely broken under all conditions. With the fixed saturation and at a lower impact velocity, the fragments were more significant in volume. As the impact velocity increased, the number of large fragments decreased, and the number of crushed powder particles gradually increased (Zhang et al. 1999). With the increase in impact velocity, the failure of the frozen sandstone was mainly transformed from tensile damage to comminuted compound fracture (Liu and Xu 2013). Under the fixed impact velocity, the number of fragments increased first and then decreased with the increase of saturation. The ratio of large-volume fragments was the highest when S was 75%. When the impact velocity exceeded 8 m/s, there were few large-volume fragments, and the fragments were mainly powder particles.
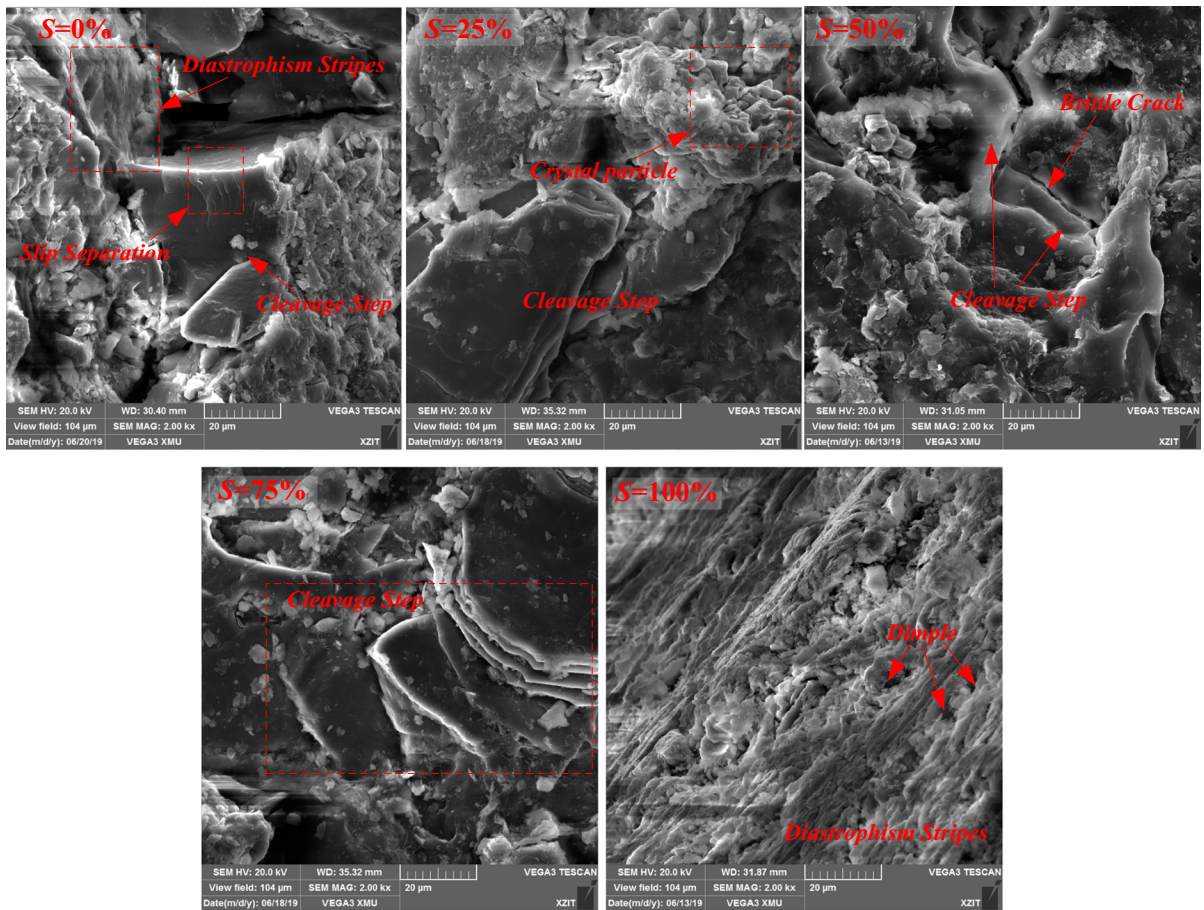
Fig. 17 Microscopic morphology of impact failure of sandstone with different saturations (2000 times)

4.1.2 Quantitative analysis of the impact failure

In Table 2, as the impact velocity increased, the overall dimension of the fragments gradually decreased, and the damage degree increased. At a fixed impact velocity, as the saturation increased, the change law of the damage degree was opposite to that of the mechanical parameters, showing the trend of first decreasing and then increasing. When S was 75%, the failure was the lowest, which was more evident at lower impact velocities. To quantitatively analyze the damage degree, the average particle size was used to quantify the change characteristics of the sandstone damage degree (Hogan et al. 2013).

Firstly, the classifying screen was used to screen the crushed specimens. The particle size ranges of the obtained particle were 0–6, 6–8.5, 8.5–11, 11–13, 13–15 and 15–30 mm, as shown in Fig. 18. 30 mm

was the particle size of the largest fragment in this test. Secondly, the fragments in each particle size range were weighed and recorded with the number of i = 1, 2, 3, 4, 5, 6. Finally, Eq. (5) was used to calculate the average particle size of the fragments, that is, the particle size coefficient r (Li et al. 2017).

$$r = \sum_{n=1}^{6} W_{iv} d_{iv} \tag{5}$$

where W_{iv} represents the percentage of the mass of the i-th group of particle size fragments to the total mass of specimens; d_{iv} is the average of the maximum particle size and the minimum particle size within the i-th group of a particle size range. r can be used to judge the average size of the whole fragments of the broken specimen and thus quantify the damage degree. That is, the more significant the r, the lower

Table 2 Failure characteristics of frozen sandstone under different saturations and impact velocities

S (%)	v (m/s)				
	6.82	7.27	7.93	8.49	8.98
0					
25					
50					
75					
100					

Fig. 18 Characteristics of fragments after the screening
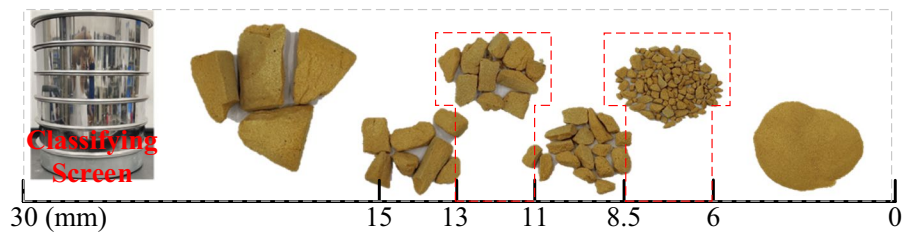
the damage degree of the sandstone, or vice versa (Li et al. 2017).

After screening and calculations, variation laws of r with S and the impact velocity v were obtained, as shown in Fig. 19. Under the fixed S, as v increased, the average r gradually decreased, indicating that the damage degree gradually increased. With the increase of S, v increased first and then decreased, representing that the damage degree first decreased and then increased. The curve fluctuations indicated that r varied greatly with different S at lower v. The maximum r was 20.74 mm with S of 75%, and the minimum was 13.13 with S of 100%. The difference was nearly 40%. With the gradual increase of v, the overall fluctuation of the curve was more minor and tended to be flat. Mainly when v exceeded 8 m/s, the saturation no longer affected the average particle size. With v of 8.98 m/s, the difference between the largest ($S = 75\%$, 9.62 mm) and the smallest particle size ($S = 100\%$, 8.06 mm) was only 16%

Fig. 19 The curved surface change of the particle size coefficient with the saturation and impact velocity
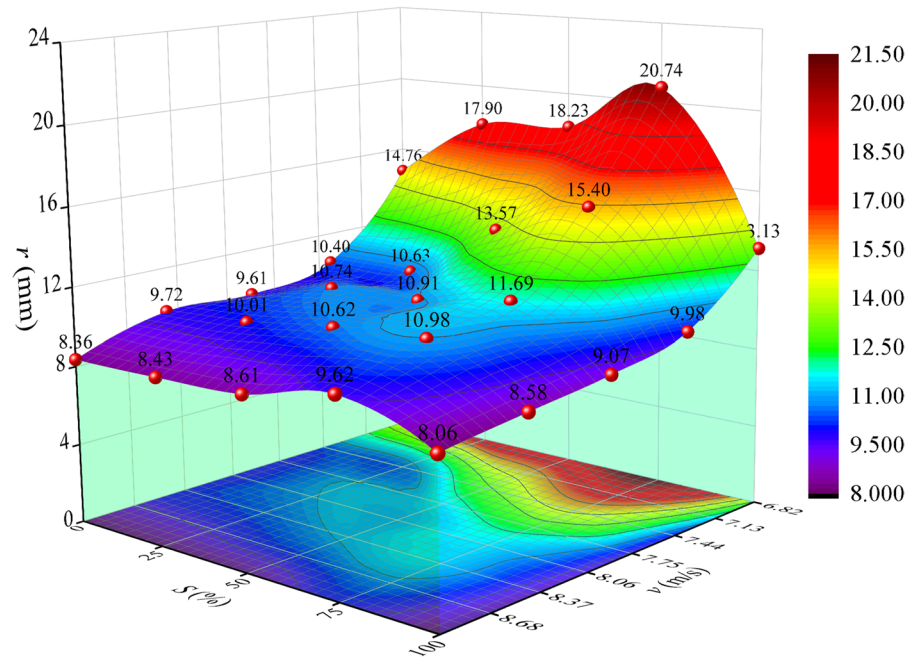
4.2 Energy dissipation mechanism of impact failure of frozen sandstone

The impact failure of frozen sandstones is a process of energy absorption and release. The initiation, expansion, and penetration of cracks until the failure of specimens are all processes of energy dissipation, which is the essence of macroscopic impact failure (Gong et al. 2021).

4.2.1 Determination and calculation method of energy dissipation parameters

There are many energy consumption parameters in the impact failure of frozen sandstone. The dissipated energy W_L and the specific surface energy λ_ω were selected in this paper (Feng et al. 2018a; Gong et al. 2019; Gao et al. 2020).

The calculation method of dissipated energy W_L was relatively simple and could be obtained by Eq. (6) using the collected strain data (Wang et al. 2018; Weng et al. 2019).

$$\begin{cases} W_{I,R,T} = E_s C_s A_s \int\limits_0^t \varepsilon_{i,r,t}(t)^2 dt \\ W_L = W_I - W_R - W_T \end{cases} \quad (6)$$

where W_I, W_R, W_T and W_L refer to the incident energy, reflected energy, transmitted energy and dissipated energy, respectively. E_s is the elastic modulus of bars of the SHPB test system; C_s is the propagation velocity of the strain wave; A_s is the diameter of the bar; ε is the strain signal collected on the bar. i, r and t represent the incident, reflection and transmission data, respectively.

The specific surface energy λ_ω refers to the surface energy of sandstone fragments per unit area, which is used to characterize the energy dissipation capacity of the fragments from the matrix. It can be calculated by Eq. (7).

$$\lambda_\omega = \frac{W_L}{S_\omega} \quad (7)$$

where S_ω is the surface area of all fragments after impact failure.

After the specimen was broken, it was tough to get the surface area of each fragment directly. Therefore, the equivalent transformation method was used to calculate the surface area S_ω of the fragment in Eq. (7).

Firstly, the crushed sandstone fragments were screened. The total mass m_i of the fragments in each particle size range could be obtained through weighing.

Secondly, the fragments in each particle size range were simplified to spheres of the average size in the particle size range, as shown in Fig. 20. Equation (8) could calculate the number of equivalent spheres in the particle size range.

$$n_i = \frac{m_i}{4\pi \rho r_i^3 / 3} \qquad (8)$$

where n_i is the total number of equivalent spheres in the i-th particle size range, and r_i is the radius of the spheres in the i-th particle size range.

Finally, the surface area of the new fragments could be calculated by Eq. (9). The first term on the right side of Eq. (9) is the surface area of all spheres, and the sum of the second term and the third term is the outer surface area of the original specimens.

$$S_\omega = \sum_{i=1}^{6} 4 n_i \pi r_i^2 - 2\pi r h - 2\pi r^2 \qquad (9)$$

where r is the radius of the sandstone specimen in the test, and h is the height of the specimen.

By substituting Eqs. (8) and (9) into Eq. (7), the specific surface energy λ_ω of frozen sandstone could be obtained during impact failure under different conditions.

4.2.2 Characteristics of dissipated energy of impact failure of frozen sandstone

According to the strain data collected by the ultra-dynamic strain gauge, the variation law of the dissipated energy W_L with v and S could be obtained by Eq. (6) during the impact, as shown in Fig. 21. Under various saturations, as v increased, the dissipation energy increased rapidly in an approximately linear form. As v increased from 6.82 to 8.98 m/s, W_L increased by 144.88%, 150.48%, 153.21%, 147.60% and 161.48%, respectively. The overall amplitude of variation was the same. After v was fixed, W_L was the largest at S of 75%, and the overall change law was consistent with that of the peak strength and dynamic elastic modulus. The fluctuation of the overall curved surface remained unchanged. In Fig. 16, as S increased from 0 to 75%, the internal morphology of the sandstone specimens became dense, and the internal cracks were reduced. During the impact process, it was necessary to provide more energy to initiate and expand new cracks. Therefore, as S increased, W_L was higher under the same input energy. While under fully saturated conditions, less energy was enough for crack expansion and penetration under the same loading conditions due to the existence of cracks and defects induced by the frost heave (Weng et al. 2019).

Fig. 20 Schematic diagram of fragments transformed into spheres after failure
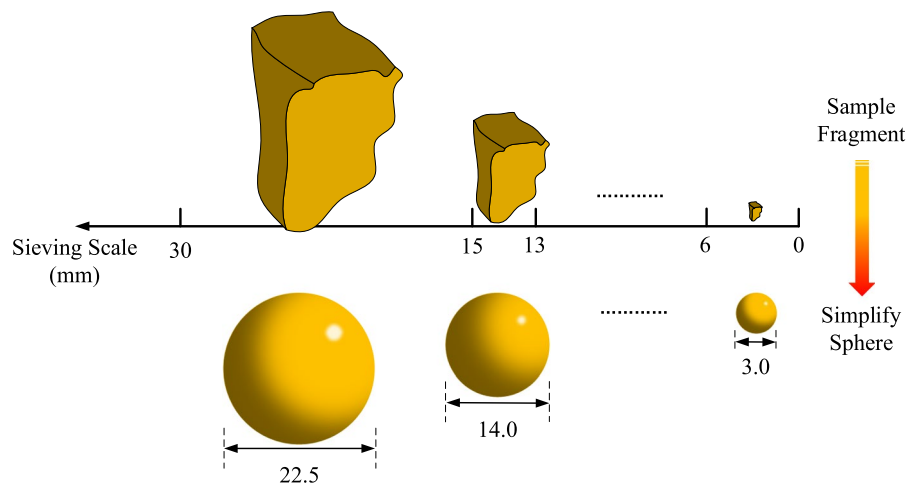
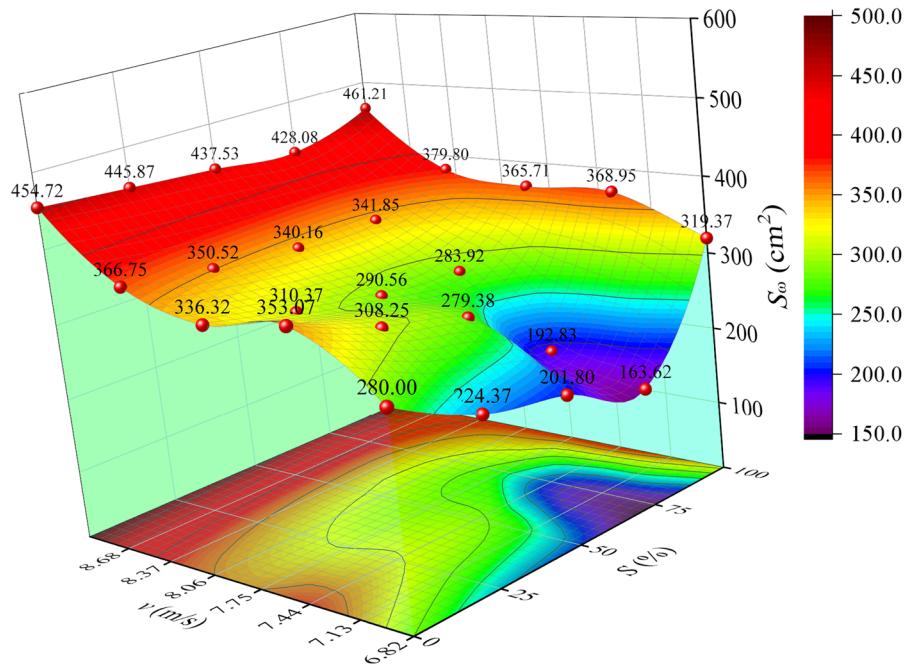**Fig. 21** Curved surface change of the dissipated energy with saturation and impact velocity
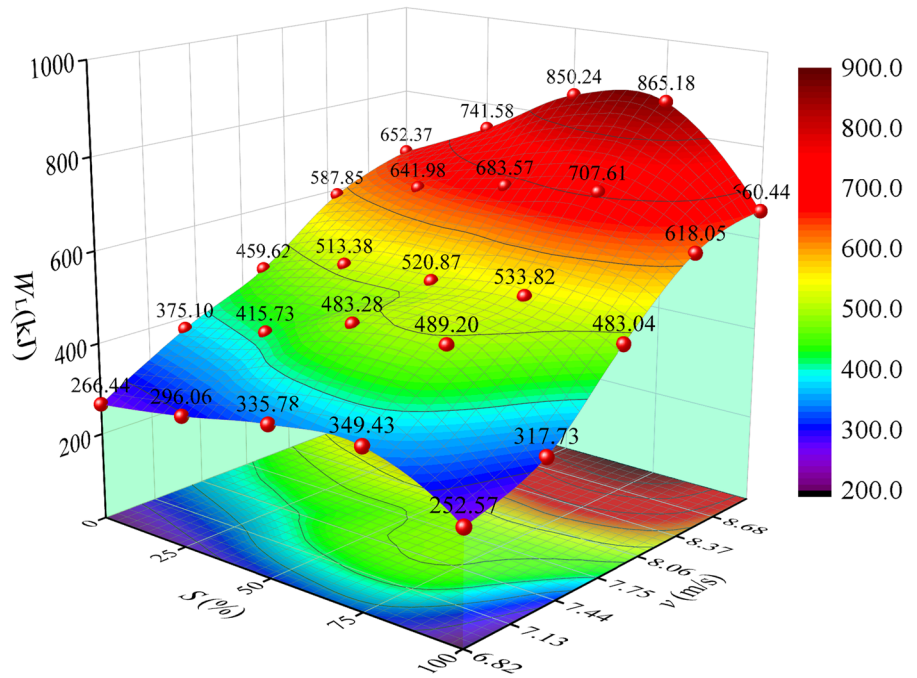
4.2.3 Characteristics of specific surface energy of sandstone fragments after impact failure

According to Eqs. (7), (8) and (9), the area S_ω and the specific surface energy λ_ω of all fragments of the

sandstone could be obtained after the impact failure. Figures 22 and 23 give the curved surfaces of S_ω and λ_ω with S and v.

In Fig. 22, as S and v increased, the change of S_ω was utterly opposite to that of the particle size

Fig. 22 Curved surface change of the area of the fragments with the saturation and the impact velocity

Fig. 23 Curved surface change of the area of the fragments with the saturation and the impact velocity
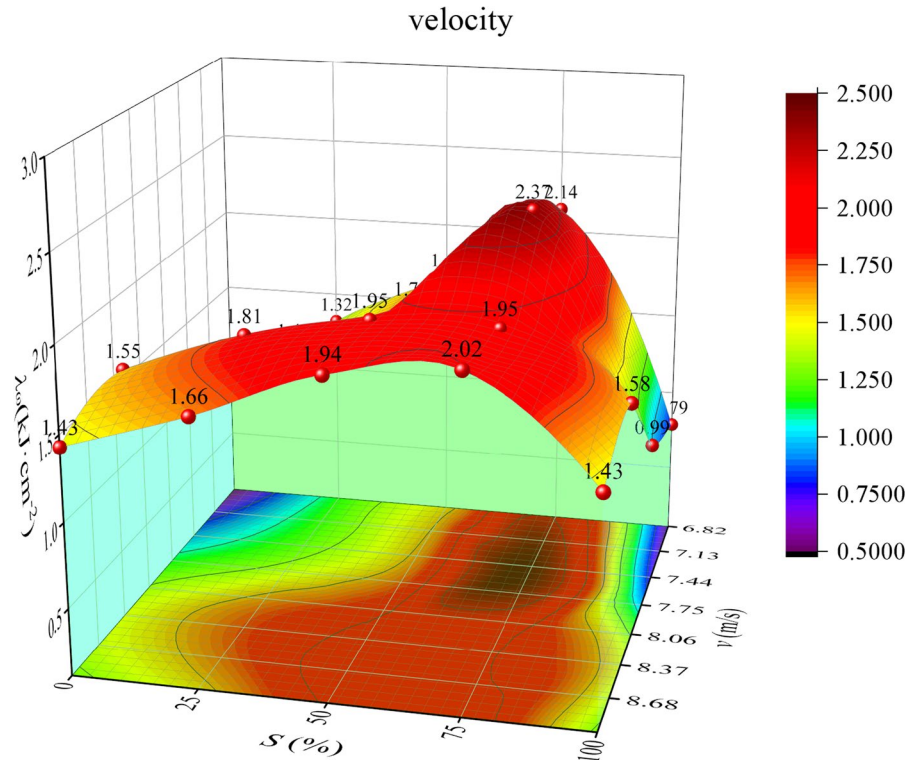
coefficient r, which also could explain the change law of the damage degree of the frozen sandstone. As v increased, S_ω increased gradually, and the increasing trend slowed down. When v exceeded 8 m/s, the change of S_ω was nearly unaffected by S. When S was 75%, S_ω was the smallest.

The variation characteristics of specific surface energy λ_ω with S and v differed from those of other mechanical and energy parameters. In Fig. 23, as v increased, λ_ω was different with various S. When S was 0%, 25%, 50% and 100%, the maximum values of λ_ω were at v of 8.49 m/s. When S was 75%, the maximum λ_ω was at v of 7.27. They were not at the place with the maximum v. This was because with a small v, the input energy was less. At this point, only those cracks that were easy to expand could absorb energy and cause visible damage to the specimen. The fragments could separate from the matrix with a small amount of energy. Thus, the specific surface energy of the whole fragments was smaller. When v and the input energy reached the maximum, a large amount of energy was consumed by lots of cracks leading to the failure of specimens. At this point, the damage degree of each fragment was even, and their

consumed energy was not the highest. New cracks occurred inside the specimens when v was at an intermediate level. The dense rock matrix was not able to timely derive cracks. The fragments separated from the matrix needed more energy for complete failure. Thus the specific surface energy was relatively high. Under a fixed v, λ_ω was the largest with S of 75%. This was also because the inside of the sandstone was dense, and more energy was needed to ensure the initiation and propagation of cracks under the same input energy.

5 Conclusions

The LT-SHPB test system was used to conduct impact loading tests for sandstone specimens with different saturations. The changes in laws of the dynamic mechanical properties of frozen sandstones were systematically analyzed. During the failure, the meso-fracture mechanism of mechanical properties and the energy dissipation mechanism were revealed. The main conclusions are given as follows:

1. The mechanical parameters of frozen sandstones had significant strain rate strengthening effects. Under the same strain rate, frozen sandstone's failure strength and elastic modulus were the largest at 75% saturation, while the peak strain was the smallest. At 75% saturation, the sensitivity of the mechanical properties to the strain rate was the strongest.

2. Frozen sandstones showed certain toughness under the actions of impact loads. At 100% saturation, the toughness was the most striking. The meso-structure characteristics showed that the mechanical properties of sandstones with low saturations exhibited significant freeze-strengthening effects in low-temperature environment. At 100% saturation, the weakening of the frost heave could be observed, which caused changes in mechanical characteristics.

3. With the increase of the impact velocity, the frozen sandstone gradually transformed from tensile failure to comminuted compound fracture, and the damage degree gradually increased. The damage degree was the lowest at 75% saturation at a fixed impact velocity.

4. During the impact failure process, the change characteristics of dissipated energy during the failure process of frozen sandstone were consistent with those of mechanical characteristic parameters. As the impact velocity increased, the damage energy consumption gradually increased. The damage energy consumption was the largest, with the same impact velocity at 75% saturation. The change characteristics of the specific surface energy of sandstone fragments were obtained by equivalent transformation. The results indicated that the energy consumption was the largest at the intermediate impact velocity for the fragments to separate from the matrix. The specific surface energy was the largest under the same impact velocity at 75% saturation.

Availability of data and materials   The data used to support the findings of this study are included in the article.

Declarations

Ethics approval and consent to participate   Ethics approval is not required for this paper.

Consent for publication   (1) That the work described has not been published before (except in the form of an abstract or as part of a published lecture, review, or thesis); (2) that it is not under consideration for publication elsewhere; (3) that its publication has been approved by all co-authors, if any; (4) that its publication has been approved (tacitly or explicitly) by the responsible authorities at the institution where the work is carried out.

Competing interests   The authors declare that they have no competing interests.

References

Ai C, Zhang J, Li Y et al (2016) Estimation criteria for rock brittleness based on energy analysis during the rupturing process. Rock Mech Rock Eng 49:4681–4698. https://doi.org/10.1007/s00603-016-1078-x

Al-Omari A, Beck K, Brunetaud X et al (2015) Critical degree of saturation: a control factor of freeze-thaw damage of porous limestones at Castle of Chambord, France. Eng Geol 185:71–80. https://doi.org/10.1016/j.enggeo.2014.11.018

Azizi A, Moomivand H (2021) A new approach to represent impact of discontinuity spacing and rock mass description on the median fragment size of blasted rocks using image analysis of rock mass. Rock Mech Rock Eng 54:2013–2038. https://doi.org/10.1007/s00603-020-02360-4

Bai Y, Shan R, Ju Y et al (2020) Study on the mechanical properties and damage constitutive model of frozen weakly cemented red sandstone. Cold Reg Sci Technol 171:102980. https://doi.org/10.1016/j.coldregions.2019.102980

Bayram F (2012) Predicting mechanical strength loss of natural stones after freeze-thaw in cold regions. Cold Reg Sci Technol 83–84:98–102. https://doi.org/10.1016/j.coldregions.2012.07.003

Cai X, Zhou Z, Tan L et al (2020) Fracture behavior and damage mechanisms of sandstone subjected to wetting-drying cycles. Eng Fract Mech 234:107109. https://doi.org/10.1016/j.engfracmech.2020.107109

Cai X, Zhou Z, Zang H, Song Z (2020) Water saturation effects on dynamic behavior and microstructure damage of sandstone: phenomena and mechanisms. Eng Geol 276:105760. https://doi.org/10.1016/j.enggeo.2020.105760

Chen L, Li K, Song G et al (2021) Effect of freeze–thaw cycle on physical and mechanical properties and damage characteristics of sandstone. Sci Rep 11:1–10. https://doi.org/10.1038/s41598-021-91842-8

Cherblanc F, Berthonneau J, Bromblet P, Huon V (2016) Influence of water content on the mechanical behaviour of limestone: role of the clay minerals content. Rock Mech Rock Eng 49:2033–2042. https://doi.org/10.1007/s00603-015-0911-y

Chi LY, Zhang Z-X, Aalberg A, Li CC (2019) Experimental investigation of blast-induced fractures in rock cylinders. Rock Mech Rock Eng 52:2569–2584. https://doi.org/10.1007/s00603-019-01749-0

Cui S, Liu P, Li Z et al (2020) Shotcrete performance-loss due to seepage and temperature coupling in cold-region tunnels. Constr Build Mater 246:118488. https://doi.org/10.1016/j.conbuildmat.2020.118488

Deng HF, Zhou ML, Li JL et al (2016) Creep degradation mechanism by water-rock interaction in the red-layer soft rock. Arab J Geosci. https://doi.org/10.1007/s12517-016-2604-6

Deprez M, De Kock T, De Schutter G, Cnudde V (2020) A review on freeze-thaw action and weathering of rocks. Earth Sci Rev 203:103143. https://doi.org/10.1016/j.earscirev.2020.103143

Dwivedi R, Soni A, Goel R, Dube A (2000) Fracture toughness of rocks under sub-zero temperature conditions. Int J Rock Mech Min Sci 37:1267–1275. https://doi.org/10.1016/S1365-1609(00)00051-4

Feng J, Wang E, Chen X, Ding H (2018a) Energy dissipation rate: an indicator of coal deformation and failure under static and dynamic compressive loads. Int J Min Sci Technol 28:397–406. https://doi.org/10.1016/j.ijmst.2017.11.006

Feng M, Wu J, Ma D et al (2018b) Experimental investigation on the seepage property of saturated broken red sandstone of continuous gradation. Bull Eng Geol Environ 77:1167–1178. https://doi.org/10.1007/s10064-017-1046-z

Gao F, Cao S, Zhou K et al (2020) Damage characteristics and energy-dissipation mechanism of frozen–thawed sandstone subjected to loading. Cold Reg Sci Technol 169:1–9. https://doi.org/10.1016/j.coldregions.2019.102920

Gong F, Yan J, Luo S, Li X (2019) Investigation on the linear energy storage and dissipation laws of rock materials under uniaxial compression. Rock Mech Rock Eng 52:4237–4255. https://doi.org/10.1007/s00603-019-01842-4

Gong F, Zhang P, Luo S et al (2021) Theoretical damage characterisation and damage evolution process of intact rocks based on linear energy dissipation law under uniaxial compression. Int J Rock Mech Min Sci 146:104858. https://doi.org/10.1016/j.ijrmms.2021.104858

Guo Y, Shen Y (2016) Agricultural water supply/demand changes under projected future climate change in the arid region of northwestern China. J Hydrol 540:257–273. https://doi.org/10.1016/j.jhydrol.2016.06.033

Hale PA, Shakoor A (2003) A laboratory investigation of the effects of cyclic heating and cooling, wetting and drying, and freezing and thawing on the compressive strength of selected sandstones. Environ Eng Geosci 9:117–130. https://doi.org/10.2113/9.2.117

Hogan JD, Castillo JA, Rawle A et al (2013) Automated microscopy and particle size analysis of dynamic fragmentation in natural ceramics. Eng Fract Mech 98:80–91. https://doi.org/10.1016/j.engfracmech.2012.11.021

Hu Y, Ma R, Wang Y et al (2019) Using hydrogeochemical data to trace groundwater flow paths in a cold alpine catchment. Hydrol Process 33:1942–1960. https://doi.org/10.1002/hyp.13440

Huang S, Liu Q, Liu Y et al (2018) Freezing strain model for estimating the unfrozen water content of saturated rock under low temperature. Int J Geomech 18:04017137. https://doi.org/10.1061/(asce)gm.1943-5622.0001057

Huang S, Ye Y, Cui X et al (2020) Theoretical and experimental study of the frost heaving characteristics of the saturated sandstone under low temperature. Cold Reg Sci Technol 174:103036. https://doi.org/10.1016/j.coldregions.2020.103036

Huang S, Cai Y, Liu Y, Liu G (2021) Experimental and theoretical study on frost deformation and damage of red sandstones with different water contents. Rock Mech Rock Eng 54:4163–4181. https://doi.org/10.1007/s00603-021-02509-9

Jaques DS, Marques EAG, Marcellino LC et al (2020) Changes in the physical, mineralogical and geomechanical properties of a granitic rock from weathering zones in a tropical climate. Rock Mech Rock Eng 53:5345–5370. https://doi.org/10.1007/s00603-020-02240-x

Jia H, Zi F, Yang G et al (2020) Influence of pore water (ice) content on the strength and deformability of frozen argillaceous siltstone. Rock Mech Rock Eng 53:967–974. https://doi.org/10.1007/s00603-019-01943-0

Jiang H, Niu F, Ma Q et al (2021) Thermal characteristics investigation of a high-speed railway tunnel by field monitoring in Northeast of China. Transp Geotech 30:100615. https://doi.org/10.1016/j.trgeo.2021.100615

Ke B, Zhou K, Xu C et al (2018) Dynamic mechanical property deterioration model of sandstone caused by freeze-thaw weathering. Rock Mech Rock Eng 51:2791–2804. https://doi.org/10.1007/s00603-018-1495-0

Ke B, Zhang C, Liu C et al (2021) An experimental study on characteristics of impact compression of freeze–thawed granite samples under four different states considering

moisture content and temperature difference. Environ Earth Sci. https://doi.org/10.1007/s12665-021-09952-5

Kim E, Changani H (2016) Effect of water saturation and loading rate on the mechanical properties of red and buff sandstones. Int J Rock Mech Min Sci 88:23–28. https://doi.org/10.1016/j.ijrmms.2016.07.005

Kodama J, Goto T, Fujii Y, Hagan P (2013) The effects of water content, temperature and loading rate on strength and failure process of frozen rocks. Int J Rock Mech Min Sci 62:1–13. https://doi.org/10.1016/j.ijrmms.2013.03.006

Li T, Song H, Huang G et al (2014) Assessment of groundwater changing trends through the generalized large well method with confined–unconfined flow model in open-pit mine area. Environ Earth Sci 72:4599–4606. https://doi.org/10.1007/s12665-014-3357-8

Li M, Mao X, Cao L et al (2016) Effects of thermal treatment on the dynamic mechanical properties of coal measures sandstone. Rock Mech Rock Eng 49:3525–3539. https://doi.org/10.1007/s00603-016-0981-5

Li M, Mao X, Cao L et al (2017) Influence of heating rate on the dynamic mechanical performance of coal measure rocks. Int J Geomech 17:04017020. https://doi.org/10.1061/(asce)gm.1943-5622.0000888

Li J, Kaunda RB, Zhou K (2018) Experimental investigations on the effects of ambient freeze-thaw cycling on dynamic properties and rock pore structure deterioration of sandstone. Cold Reg Sci Technol 154:133–141. https://doi.org/10.1016/j.coldregions.2018.06.015

Li F, Zhao K, Lu H et al (2021a) Modes of exploitation of atmospheric water resources in the Qinghai–Tibet plateau. Int J Climatol 41:3237–3246. https://doi.org/10.1002/joc.7016

Li Y, Zhai Y, Meng F, Zhang Y (2021b) Study on the influence of freeze-thaw weathering on the mechanical properties of Huashan granite strength. Rock Mech Rock Eng 54:4741–4753. https://doi.org/10.1007/s00603-021-02497-w

Lifshitz JM, Leber H (1994) Data processing in the split Hopkinson pressure bar tests. Int J Impact Eng 15:723–733. https://doi.org/10.1016/0734-743X(94)90011-9

Lin G, Li M, Chen Y et al (2021) Dynamic tensile mechanical properties and fracture characteristics of water-saturated sandstone under the freezing effect. Int J Geomech 21:04021044. https://doi.org/10.1061/(asce)gm.1943-5622.0001999

Liu S, Xu J (2013) Study on dynamic characteristics of marble under impact loading and high temperature. Int J Rock Mech Min Sci 62:51–58. https://doi.org/10.1016/j.ijrmms.2013.03.014

Liu SL, Chen HR, Yuan SS, Zhu QZ (2020) Experimental investigation and micromechanical modeling of the brittle-ductile transition behaviors in low-porosity sandstone. Int J Mech Sci 179:105654. https://doi.org/10.1016/j.ijmecsci.2020.105654

Liu Y, Cai Y, Huang S et al (2020b) Effect of water saturation on uniaxial compressive strength and damage degree of clay-bearing sandstone under freeze-thaw. Bull Eng Geol Environ 79:2021–2036. https://doi.org/10.1007/s10064-019-01686-w

Luo Y, Qu D, Wang G et al (2020) Degradation model of the dynamic mechanical properties and damage failure law of sandstone under freeze-thaw action. Soil Dyn Earthq Eng 132:106094. https://doi.org/10.1016/j.soildyn.2020.106094

Ma Q, Ma D, Yao Z (2018) Influence of freeze-thaw cycles on dynamic compressive strength and energy distribution of soft rock specimen. Cold Reg Sci Technol 153:10–17. https://doi.org/10.1016/j.coldregions.2018.04.014

Ming F, Zhang S, Niu F, Zhou Z (2021) A study on crack damage stress and the damage constitutive model of frozen sandstone. Bull Eng Geol Environ 80:6955–6970. https://doi.org/10.1007/s10064-021-02361-9

Navarro Torres VF, Silveira LGC, Lopes PFT, de Lima HM (2018) Assessing and controlling of bench blasting-induced vibrations to minimize impacts to a neighboring community. J Clean Prod 187:514–524. https://doi.org/10.1016/j.jclepro.2018.03.210

Qi S, Yue ZQ, Wu F, Chang Z (2009) Deep weathering of a group of thick argillaceous limestone rocks near Three Gorges Reservoir, Central China. Int J Rock Mech Min Sci 46:929–939. https://doi.org/10.1016/j.ijrmms.2009.03.006

Seyed Mousavi SZ, Tavakoli H, Moarefvand P, Rezaei M (2019) Assessing the effect of freezing-thawing cycles on the results of the triaxial compressive strength test for calc-schist rock. Int J Rock Mech Min Sci 123:104090. https://doi.org/10.1016/j.ijrmms.2019.104090

Shang Y, Park H-D, Yang Z, Zhang L (2004) Debris formation in Southeast Tibet from weathering, avalanching, rock falling and mass movement. Int J Rock Mech Min Sci 41:528–529. https://doi.org/10.1016/j.ijrmms.2003.12.112

Shen Y, Shen Y, Guo Y et al (2020) Review of historical and projected future climatic and hydrological changes in mountainous semiarid Xinjiang (northwestern China), central Asia. CATENA 187:104343. https://doi.org/10.1016/j.catena.2019.104343

Song Y, Tan H, Yang H et al (2021) Fracture evolution and failure characteristics of sandstone under freeze-thaw cycling by computed tomography. Eng Geol 294:106370. https://doi.org/10.1016/j.enggeo.2021.106370

Takarli M, Prince W, Siddique R (2008) Damage in granite under heating/cooling cycles and water freeze–thaw condition. Int J Rock Mech Min Sci 45:1164–1175. https://doi.org/10.1016/j.ijrmms.2008.01.002

Tan X, Chen W, Liu H et al (2018) A unified model for frost heave pressure in the rock with a penny-shaped fracture during freezing. Cold Reg Sci Technol 153:1–9. https://doi.org/10.1016/j.coldregions.2018.04.016

Tarasov B, Potvin Y (2013) Universal criteria for rock brittleness estimation under triaxial compression. Int J Rock Mech Min Sci 59:57–69. https://doi.org/10.1016/j.ijrmms.2012.12.011

Walton G (2021) A new perspective on the brittle-ductile transition of rocks. Rock Mech Rock Eng. https://doi.org/10.1007/s00603-021-02595-9

Wang P, Xu J, Liu S et al (2016a) Static and dynamic mechanical properties of sedimentary rock after freeze-thaw or thermal shock weathering. Eng Geol 210:148–157. https://doi.org/10.1016/j.enggeo.2016.06.017

Wang P, Xu J, Liu S et al (2016b) A prediction model for the dynamic mechanical degradation of sedimentary rock after a long-term freeze-thaw weathering: Considering the

strain-rate effect. Cold Reg Sci Technol 131:16–23. https://doi.org/10.1016/j.coldregions.2016.08.003

Wang P, Xu J, Fang X, Wang P (2017) Energy dissipation and damage evolution analyses for the dynamic compression failure process of red-sandstone after freeze-thaw cycles. Eng Geol 221:104–113. https://doi.org/10.1016/j.enggeo.2017.02.025

Wang ZL, Shi H, Wang JG (2018) Mechanical behavior and damage constitutive model of granite under coupling of temperature and dynamic loading. Rock Mech Rock Eng 51:3045–3059. https://doi.org/10.1007/s00603-018-1523-0

Wang C, Li S, Zhang T, You Z (2019a) Experimental study on mechanical characteristics and fracture patterns of unfrozen/freezing saturated coal and sandstone. Materials (Basel) 12:992. https://doi.org/10.3390/ma12060992

Wang Y, Yang Y, Zhang Y, Wang J (2019b) Dynamic mechanical properties of coals subject to the low temperature-impact load coupling effect. Sci Rep 9:1–13. https://doi.org/10.1038/s41598-019-56755-7

Wang Z, Zhu Z, Zhu S (2019c) Thermo-mechanical-water migration coupled plastic constitutive model of rock subjected to freeze-thaw. Cold Reg Sci Technol 161:71–80. https://doi.org/10.1016/j.coldregions.2019.03.001

Wang S, Zhao W, Fu X et al (2020) A universal method for quantitatively evaluating rock brittle-ductile transition behaviors. J Pet Sci Eng. https://doi.org/10.1016/j.petrol.2020.107774

Wang ZL, Hao SY, Zheng J et al (2020b) Study on energy properties and failure behaviors of heat-treated granite under static and dynamic compression. Mech Adv Mater Struct 27:462–472. https://doi.org/10.1080/15376494.2018.1479808

Wang T, Sun Q, Jia H et al (2021a) Linking the mechanical properties of frozen sandstone to phase composition of pore water measured by LF-NMR at subzero temperatures. Bull Eng Geol Environ 80:4501–4513. https://doi.org/10.1007/s10064-021-02224-3

Wang W, Yao Q, Tang C et al (2021) Experimental study on the shear characteristics and weakening mechanism of water-bearing rock joints. Bull Eng Geol Environ. https://doi.org/10.1007/s10064-021-02390-4

Weng L, Wu Z, Liu Q, Wang Z (2019) Energy dissipation and dynamic fragmentation of dry and water-saturated siltstones under sub-zero temperatures. Eng Fract Mech. https://doi.org/10.1016/j.engfracmech.2019.106659

Weng L, Wu Z, Liu Q (2020) Dynamic Mechanical properties of dry and water-saturated siltstones under sub-zero temperatures. Rock Mech Rock Eng 53:4381–4401. https://doi.org/10.1007/s00603-019-02039-5

Weng L, Wu Z, Liu Q et al (2021) Evolutions of the unfrozen water content of saturated sandstones during freezing process and the freeze-induced damage characteristics. Int J Rock Mech Min Sci 142:104757. https://doi.org/10.1016/j.ijrmms.2021.104757

Xia K, Yao W (2015) Dynamic rock tests using split Hopkinson (Kolsky) bar system: a review. J Rock Mech Geotech Eng 7:27–59. https://doi.org/10.1016/j.jrmge.2014.07.008

Xie H, Li L, Ju Y et al (2011) Energy analysis for damage and catastrophic failure of rocks. Sci China Technol Sci 54:199–209. https://doi.org/10.1007/s11431-011-4639-y

Xu Y, Dai F (2018) Dynamic response and failure mechanism of brittle rocks under combined compression-shear loading experiments. Rock Mech Rock Eng 51:747–764. https://doi.org/10.1007/s00603-017-1364-2

Xue L, Qin S, Sun Q et al (2014) A study on crack damage stress thresholds of different rock types based on uniaxial compression tests. Rock Mech Rock Eng 47:1183–1195. https://doi.org/10.1007/s00603-013-0479-3

Yang R, Fang S, Guo D et al (2019) Study on dynamic tensile strength of red sandstone under impact loading and negative temperature. Geotech Geol Eng 37:4527–4537. https://doi.org/10.1007/s10706-019-00927-9

Yin T, Li X, Cao W, Xia K (2015) Effects of thermal treatment on tensile strength of Laurentian granite using Brazilian test. Rock Mech Rock Eng 48:2213–2223. https://doi.org/10.1007/s00603-015-0712-3

Zhang QB, Zhao J (2014) A review of dynamic experimental techniques and mechanical behaviour of rock materials. Rock Mech Rock Eng 47:1411–1478. https://doi.org/10.1007/s00603-013-0463-y

Zhang ZX, Kou SQ, Jiang LG, Lindqvist P-A (1999) Effects of loading rate on rock fracture: fracture characteristics and energy partitioning. Int J Rock Mech Min Sci 36:597–611. https://doi.org/10.1016/S0148-9062(99)00031-5

Zhang J, Deng H, Taheri A et al (2018) Degradation of physical and mechanical properties of sandstone subjected to freeze-thaw cycles and chemical erosion. Cold Reg Sci Technol 155:37–46. https://doi.org/10.1016/j.coldregions.2018.07.007

Zhang M, Wen Z, Li D et al (2021) Impact process and mechanism of summertime rainfall on thermal–moisture regime of active layer in permafrost regions of central Qinghai-Tibet Plateau. Sci Total Environ 796:148970. https://doi.org/10.1016/j.scitotenv.2021.148970

Zhou YX, Xia K, Li XB et al (2012) Suggested methods for determining the dynamic strength parameters and mode-I fracture toughness of rock materials. Int J Rock Mech Min Sci 49:105–112. https://doi.org/10.1016/j.ijrmms.2011.10.004

Zhou KP, Li B, Li JL et al (2015) Microscopic damage and dynamic mechanical properties of rock under freeze-thaw environment. Trans Nonferrous Met Soc China (Engl Ed) 25:1254–1261. https://doi.org/10.1016/S1003-6326(15)63723-2

Zhou W, Shi X, Lu X et al (2020) The mechanical and microstructural properties of refuse mudstone-GGBS-red mud based geopolymer composites made with sand. Constr Build Mater 253:119193. https://doi.org/10.1016/j.conbuildmat.2020.119193

Zhou XP, Li CQ, Zhou LS (2020) The effect of microstructural evolution on the permeability of sandstone under freeze-thaw cycles. Cold Reg Sci Technol 177:103119. https://doi.org/10.1016/j.coldregions.2020.103119

Zhou Z, Yude E, Cai X, Zhang J (2021) Coupled effects of water and low temperature on quasistatic and dynamic mechanical behavior of sandstone. Geofluids 2021:10. https://doi.org/10.1155/2021/9926063